J Toxicol Pathol 2013; 26: 231–257

Report

Proceedings of the 2013 Joint JSTP/NTP Satellite Symposium

Susan A. Elmore[1*], Mark Hoenerhoff[1], Osamu Katsuta[2], Hiroko Kokoshima[3], Robert Maronpot[4], Hiroaki Nagai[5], Hiroshi Satoh[6], Yasuhiro Tanaka[7], Tomoaki Tochitani[8], Seiichiro Tsuchiya[9], and Katsuhiko Yoshizawa[10]

[1] National Toxicology Program, National Institute of Environmental Health Sciences, National Institutes of Health, 111 T.W. Alexander Drive, Research Triangle Park, North Carolina 27709, USA
[2] Santen Pharmaceutical Co., Ltd., Ikoma, Nara 630-0101, Japan
[3] Mitsubishi Chemical Medience Corp., 14-1 Sunayama, Kamisu, Ibaraki 314-0255, Japan
[4] Maronpot Consulting LLC, Raleigh, North Carolina, USA
[5] Nihon Nohyaku Co., Ltd., 345 Oyamada-cho, Kawachi-Nagano, Osaka 586-0094, Japan
[6] Safety Evaluation Center, Fujifilm Corp., 210 Nakanuma, Minamiashigara, Kanagawa 250-0193, Japan
[7] Faculty of Pharmaceutical Sciences, Setsunan University, 45-1 Nagaotoge, Hirakata, Osaka 573-0101, Japan
[8] Dainippon Sumitomo Pharma Co., Ltd., 3-1-98 Kasugade-naka, Konohana-ku, Osaka 554-0022, Japan
[9] Ishihara Sangyo Kaisha, Ltd., 2-3-1 Nishi-Shibukawa, Kusatsu, Shiga 525-0025, Japan
[10] Kansai Medical University, 2-5-1 Shinmachi, Hirakata, Osaka 573-1010, Japan

Abstract: The first joint Japanese Society of Toxicologic Pathology (JSTP) and National Toxicology Program (NTP) Satellite Symposium, entitled "Pathology Potpourri," was held on January 29th at Okura Frontier Hotel in Tsukuba, Ibaraki, Japan, in advance of the JSTP's 29th Annual Meeting. The goal of this Symposium was to present current diagnostic pathology or nomenclature issues to the toxicologic pathology community. This article presents summaries of the speakers' presentations, including diagnostic or nomenclature issues that were presented, select images that were used for audience voting or discussion, and the voting results. Some lesions and topics covered during the symposium include: treatment-related atypical hepatocellular foci of cellular alteration in B6C3F1 mice; purulent ventriculoencephalitis in a young BALB/c mouse; a subcutaneous malignant schwannoma in a RccHan:WIST rat; spontaneous nasal septum hyalinosis/eosinophilic substance in B6C3F1 mice; a rare pancreatic ductal cell adenoma in a young Lewis rat; eosinophilic crystalline pneumonia in a transgenic mouse model; hyaline glomerulopathy in two female ddY mice; treatment-related intrahepatic erythrocytes in B6C3F1 mice; treatment-related subendothelial hepatocytes in B6C3F1 mice; spontaneous thyroid follicular cell vacuolar degeneration in a cynomolgus monkey; congenital hepatic fibrosis in a 1-year-old cat; a spontaneous adenocarcinoma of the middle ear in a young Crl:CD(SD) rat; and finally a series of cases illustrating some differences between cholangiofibrosis and cholangiocarcinoma in Sprague Dawley and F344 rats. (DOI: 10.1293/tox.26.231; J Toxicol Pathol 2013; 26: 231–257)

Key words: JSTP/NTP Satellite Symposium, atypical foci of cellular alteration, cholangiocarcinoma, cholangiofibrosis, congenital hepatic fibrosis, eosinophilic crystalline pneumonia, eosinophilic substance, epithelioid type of malignant schwannoma, hyaline glomerulopathy, intrahepatocytic erythrocytes, middle ear adenocarcinoma, nasal septum hyalinosis, pancreatic ductal cell adenoma, subendothelial hepatocytes, thyroid follicular cell vacuolar degeneration, ventriculoencephalitis

Introduction

The first JSTP/NTP Satellite Symposium was a one-day meeting held in conjunction with the annual JSTP meeting, entitled "The Future of Toxicologic Pathology in the Post-Genomic Era," in Tsukuba, Japan. This joint meeting was fashioned after the very popular annual NTP Satellite Symposium that is traditionally held in advance of the annual Society of Toxicologic Pathology (STP) meeting[1–4]. The objective of this symposium is to provide continuing education concerning interpretation of histopathology slides. This includes the presentation and discussion of diagnostically difficult lesions, interesting or rare lesions, or challenging nomenclature issues. The session is interactive in that each speaker presents images for audience voting via wireless keypads. Once the votes are tallied, the results are displayed on the screen for audience members to view. The speaker generally provides his or her preferred diagnosis for comparison with some additional background information, after which audience discussion occurs.

The theme for this Symposium was "Pathology Potpourri," which allowed for a variety of topics to be presented. Species included the rat, mouse and monkey. Organ

Received: 31 March 2013, Accepted: 4 April 2013
*Corresponding author: SA Elmore (e-mail: elmore@niehs.nih.gov)

systems/tissues included the liver, brain, pancreas, kidney, thyroid, lung, subcutis, nasal septum, and middle ear. Dr. Takanori Harada (The Institute of Environmental Toxicology, Ibaraki, Japan), president of the annual meeting of the JSTP, provided the welcome and introductory remarks. Drs. Susan Elmore and Katsuhiko Yoshizawa co-chaired the meeting. Dr. Bob Maronpot ended the symposium with a comprehensive review of proliferative cholangial lesions and the historical difficulties in diagnosing cholangiofibrosis and cholangiocarcinoma. This article provides synopses of all presentations including the diagnostic or nomenclature issues, a selection of images presented for voting and discussion, voting choices, voting results, and major discussion points.

Focus of Cellular Alteration, Atypical

Dr. Susan Elmore of the NTP and NIEHS presented the first case of the JSTP/NTP Joint Symposium. This was an unusual liver lesion seen in male and female B6C3F1 mice from a dosed water NTP carcinogenicity bioassay, which is still under study. After showing a series of low- and high-magnification images (Figs. 1A–F), the audience was asked to vote. The voting choices and results were focus of cellular alteration (3%); focus of cellular alteration, atypical (36%); focus of hypertrophied hepatocytes, cellular atypia (16%); focus of hyperplastic hepatocytes, cellular atypia (19%); hepatocellular nodular hyperplasia (3%); hepatocellular dysplasia (3%); hepatocellular adenoma (8%); and hepatocellular carcinoma (11%). This same lesion was presented at the 2012 NTP Satellite Symposium, and two favored diagnoses were focus of cellular alteration, atypical (34%), and focus of hypertrophied hepatocytes, cellular atypia (37%)[1].

The NTP diagnosed this lesion as "focus of cellular alteration, atypical," similar to 36% of the audience members. Cellular atypia was considered by 71% of the audience to be a component of the diagnosis as opposed to a neoplastic process. In this study, the cellular atypia was only identified within eosinophilic and mixed cell foci, which was difficult to portray in the projected images. The foci occurred as single or multifocal nodular aggregates that merged with the surrounding parenchyma and occasionally caused slight compression of surrounding tissue (Fig. 1G). Cellular features included cytomegaly, karyomegaly, intranuclear invaginations, multiple prominent nucleoli and intracytoplasmic and intranuclear vacuoles (Fig. 1H).

This lesion was present in mouse one- and two-year bioassays, was not present in 13- or 26-week studies, and was not present in rats. In the mouse one- and two-year studies, there was a remarkable treatment-related increase in this lesion in both male and female mice (Table 1). There were also increased incidences of liver neoplasia in male and female mice in the one-year bioassay; hepatocellular carcinoma, including multiples, and hepatoblastomas. However, hepatocellular adenomas and foci of cellular alteration were not significantly increased (data not shown). In the two-year bioassay, there were also increased incidences of liver neoplasia in male and female mice; hepatocellular carcinomas including multiples, hepatoblastomas including multiples and hepatocellular cholangiocarcinomas. As in the one-year study, hepatocellular adenomas and foci of cellular alteration were not significantly increased (data not shown).

For this study, the pathologists diagnosed atypical hyperplastic foci only if there was pronounced karyomegaly and cytomegaly within eosinophilic or mixed cell foci, regardless of whether or not there were intranuclear inclusions or other atypical features. The atypical foci were not considered adenomas or carcinomas because they lacked these features: well-circumscribed, distinct compression and invasion, abnormal growth pattern, necrosis, hemorrhage, or metastases.

Dr. Elmore indicated that there are no other reported studies with karyomegaly or other features of cellular atypia within foci of cellular alteration. If preneoplastic, then this unique treatment-related lesion appears to bypass the normal adenoma phase of hepatocarcinogenesis. Therefore, additional mechanistic studies are needed to clarify the pathogenesis of this lesion.

Table 1. Incidences of "Focus of Cellular Alteration, Atypical" in Treated B6C3F1 Mice

	Control	Low Dose	Mid Dose	High Dose
One-Year Study[+]				
Males	0**	2	4	6**
Females	0*	2	3	4*
Two-Year Study[++]				
Males	0**	19**	42**	43**
Females	0**	2	6*	16**

+ 7–8 animals per group. ++ 49–51 animals per group. *$p \leq 0.05$; **$p \leq 0.01$; Cochran-Armitage trend test and Fisher's exact test.

Fig. 1. Focus of atypical cellular alteration in treated B6C3F1 mice. A: Focus of atypical cellular alteration from a 2-year bioassay showing an irregular boundary. B: Higher magnification of 1A showing cytomegaly, karyomegaly, and intranuclear invaginations. C: Another focus of cellular alteration showing the irregularity of the cell boundary. D: Higher magnification of 1C showing the edge of the lesion. Compared with the normal hepatocytes (upper left), there is cellular atypia with marked cytomegaly and karyomegaly with nuclear invaginations. E: Focus of atypical cellular alteration from a 1-year bioassay (arrow). Compared with the 2-year bioassay, the focus is smaller with a more well-defined cell border. F: Higher magnification of 1E showing the cellular hypertrophy and karyomegaly. G: High magnification of an atypical focus from a 2-year bioassay showing minimal compression with the adjacent normal parenchyma. H: High magnification of an atypical focus from a 2-year bioassay showing intracytoplasmic and intranuclear clear round vacuoles with sharp borders. There is also intranuclear invagination of the cytoplasm in a few of the cells.

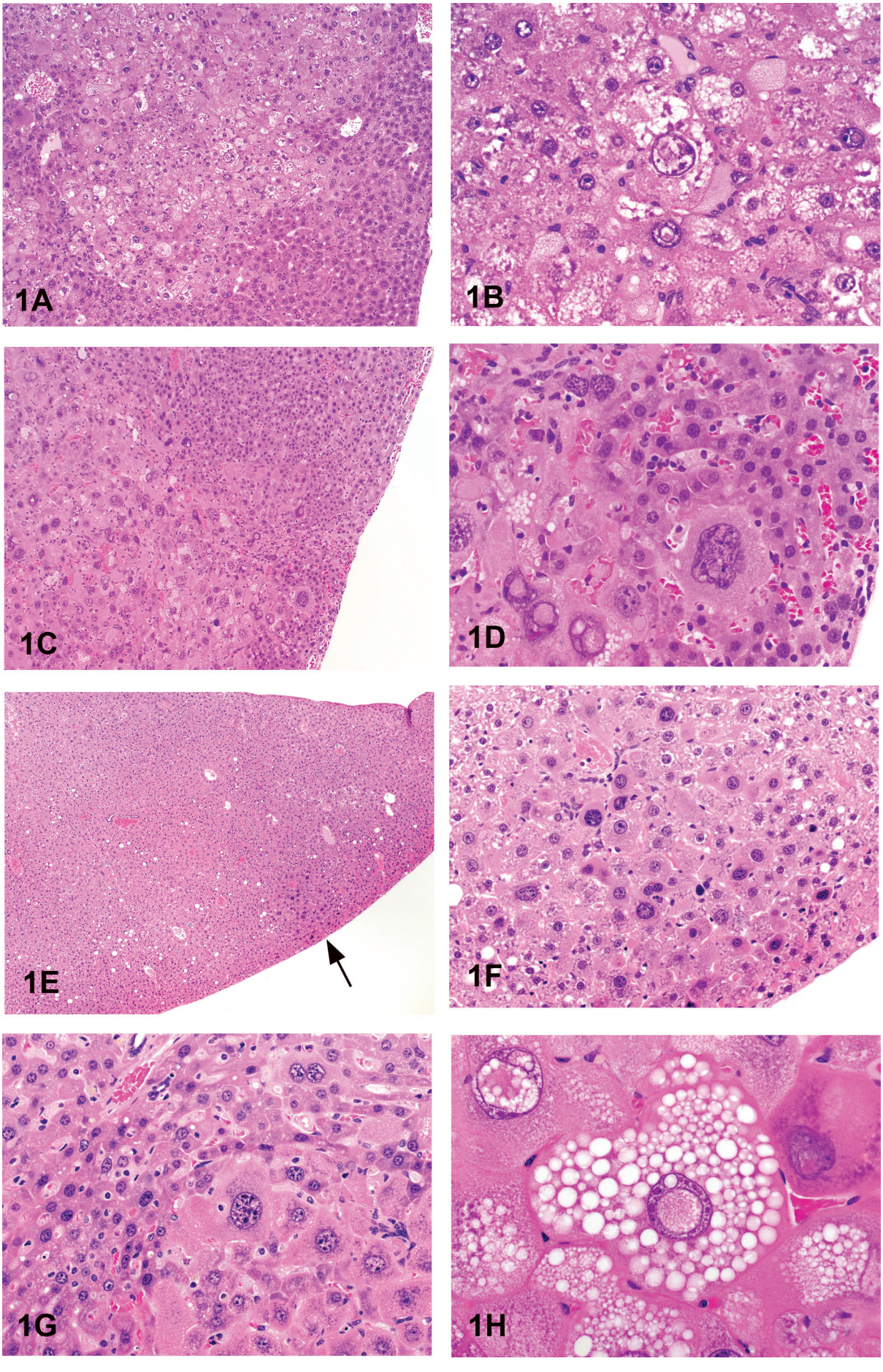
1A
1B
1C
1D
1E
1F
1G
1H

Ventriculoencephalitis in a Young Mouse

Dr. Osamu Katsuta of Santen Pharmaceutical Co., Ltd. presented "A Brain Lesion in a Young Mouse." One of 60 male BALB/c mice, 5 weeks old, suddenly showed neurologic signs such as torticollis and circling on day 3 of an acclimation/quarantine period. The animal was sacrificed under anesthesia the next day. At necropsy, the right hemisphere of the brain was slightly swollen. The brain and both eyes were collected for histopathology.

The brain lesion was mainly confined to the ventricles. The 3rd and lateral ventricles contained pyogenic debris (Fig. 2A). In the parenchyma near the ventricle, hyaline thrombi, necrotic neurons and glial cells were present, along with parenchymal swelling (Fig. 2B). Also, pyogenic debris was observed in the 4th ventricle. Neutrophils and some foam cells had engulfed minute granular material within their cytoplasm (Fig. 2C). This material was positive with Gram staining and was identified as *Staphylococcus aureus* by immunohistochemistry using anti-*S. aureus* antibody (Biodesign International, Saco, ME, USA) (Fig. 2D). The bacteria were detected only in the ventricles. The symposium participants were asked to vote on a number of diagnoses: brain abscess, purulent encephalitis, purulent ventriculoencephalitis, granulomatous ventriculoencephalitis, and necrotizing ventriculoencephalitis. The vote was overwhelming for purulent ventriculoencephalitis (65%), which agreed with the speaker's diagnosis.

Discussion points were 1) characteristic findings in this case, 2) distribution of the findings and 3) the origin of the bacteria. Some of the characteristic features in this case included suppurative inflammation, edematous changes in the parenchyma near the ventricle, vascular hyalinization with small hemorrhages and single cell necrosis of neurons or glial cells. Surrounding the ventricle, there was a weak positive reaction in immunostaining for glial fibrillary acidic protein (GFAP, DakoCytomation Denmark A/S, Glostrup, Denmark) (Fig. 2E), possibly because of bacterial endotoxin. Few macrophages were seen near the ventricle, and microglial cells were diffusely observed in the parenchyma (Fig. 2F) by immunostaining of Iba-1 (Wako, Osaka, Japan). Pyogenic changes were limited to, or near, the ventricles. Therefore, this change may be distributed to the spinal cord. However, to our regret, the spinal cord was not collected at necropsy. In humans, ventriculoencephalitis is the most common form of cytomegalovirus infection in the CNS of immunocompromised patients[5, 6]. One of the members of the Kansai Conference on Toxicologic Pathology (KCTP) has identified a purulent ventriculitis in a Chinchilla cat. In addition, one audience member noted that in rodents, bacteria in the submandibular gland or parotid gland sometimes invades the CNS and can cause ventriculitis. Determining the origin of the bacteria was challenging. Only one mouse was affected. According to the breeder, the same symptom did not occur within the colony, so this was an isolated event. One important characteristic of maternal behavior is that the mother mouse takes her pup's neck into her mouth for transportation purposes. However, the suture of the skull does not close until 2 or 3 weeks after birth in mice (author's experience). It is possible that the bacteria invaded from the suture of the skull as a result of being carried by the mother, entered the brain, and proliferated within the ventricles. In this way, the bacteria would not have to cross the blood brain barrier. During the discussion, one audience member commented that a scar from the bite might have been left on the neck skin in this case. Although we were not aware of any gross changes, except the head deformation, the skin lesion might have been overlooked at necropsy. We will need to accumulate similar cases in order to confirm the external bacterial invasion theory.

A Subcutaneous Epithelioid Type of Malignant Schwannoma in a RccHan:WIST Rat

Dr. Seiichiro Tsuchiya of Ishihara Sangyo Kaisha, Ltd. presented a case of a subcutaneous tumor in a female rat. This subcutaneous tumor arose at the right buccal region in a 93-week-old female RccHan™: WIST rat that was kept in a historical background data collection study. This animal showed wryneck and abnormal gait with a progressively worsening general condition. At necropsy and histopathological examination, several findings were observed, such as a pituitary mass (adenoma, pars distalis), a thyroid nodule (follicular cell adenoma) and an accentuated lobular pattern and red spot on the liver (hepatocellular fatty change and foci of eosinophilic cellular alteration, respectively). However, these findings were considered unrelated to this tumor.

The subcutaneous mass was a solitary nodule that was approximately 1 × 0.8 cm in size, with surface flaking and scabbing. Histopathologically, it was completely encapsulated by connective tissue with no connection to the overlying skin epithelium (Fig. 3A). At high magnification, the tumor cells were densely packed, polygonal to spindle shaped, with well-defined cell borders and abundant eosinophilic cytoplasm. Nuclei were oval to round with prominent nucleoli. Mitotic figures were occasionally observed, indicating that this tumor had a high proliferative activity (Fig. 3B). To confirm the origin of this tumor, immunohistochemistry was performed using cytokeratin (Fig. 3C), vimentin (Fig. 3D), S-100 (Fig. 3E), Schwann/peripheral myelin (Fig. 3F) and CD68 antibodies. The results are shown in Table 2. A positive reaction was obtained with vimentin, S-100 and Schwann/peripheral myelin, whereas a negative reaction was seen with cytokeratin and CD68. These results, taken together, suggest that the origin of this tumor was a neural cell, specifically a Schwann cell. From the hematoxylin & eosin (H&E) findings and immunohistochemical results, the possibility of a melanoma was considered.

To differentiate between schwannoma and melanoma, further examinations were performed. These two tumor types can be differentiated based on the presence of a basal lamina (schwannoma) or premelanosomes (melanoma). PAS, silver impregnation stain and electron microscopy were performed. In the PAS reaction and silver impregnation stain-

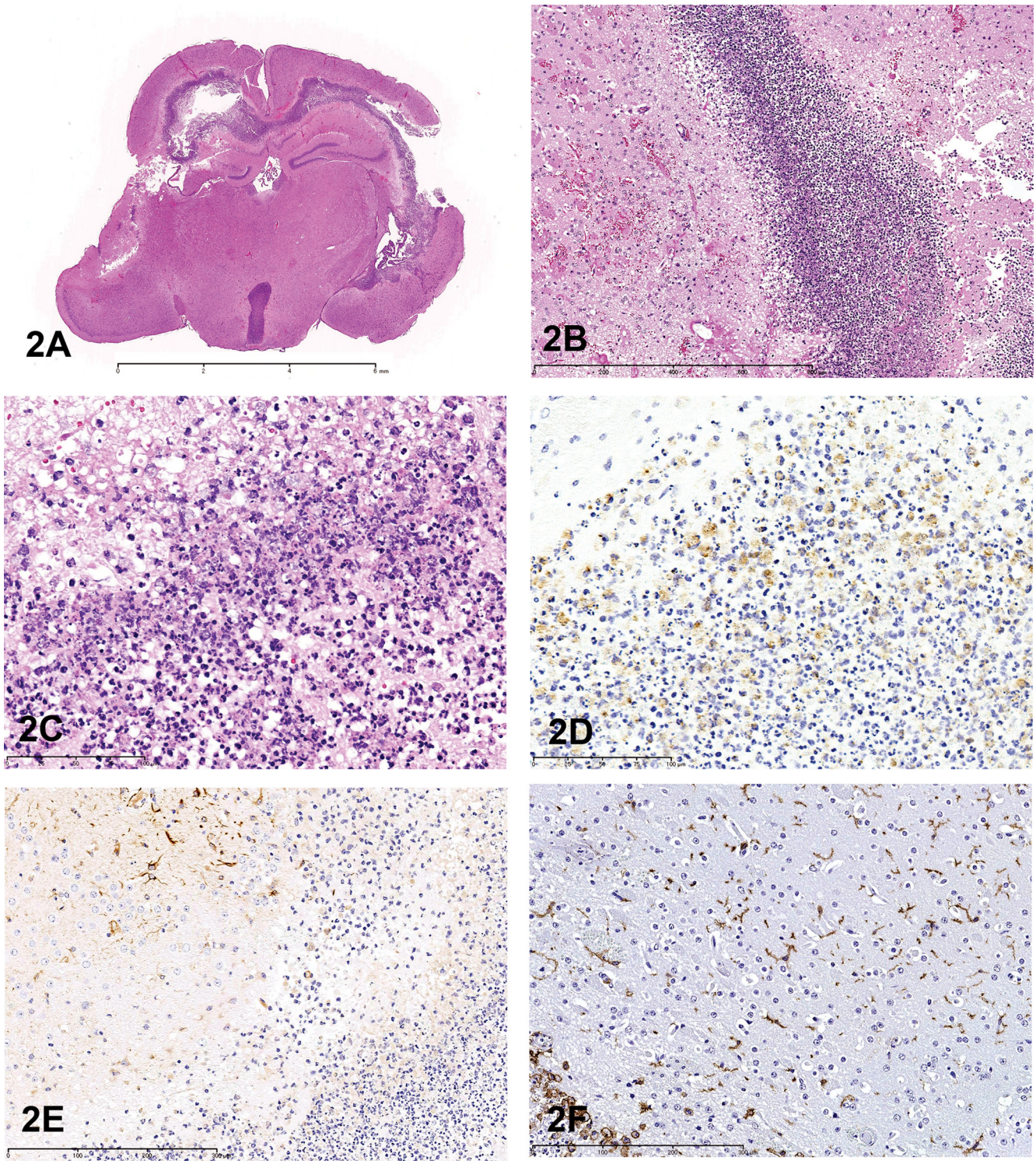

Fig. 2. Purulent ventriculoencephalitis in a young BALB/c mouse. A: The ventricles are mainly affected. Cortical malacia is observed adjacent to the lateral ventricle. H & E staining, × 5. B: The parenchyma near the ventricle. Edema, and vascular hyalinization with small hemorrhage are detected. H & E staining, × 100. C: Neutrophils and some foam cells engulf minute granular materials in their cytoplasm. H & E staining, × 400. D: Immunohistochemistry for *Staphylococcus aureus*. The cytoplasm in neutrophils and macrophages react positively for anti-*S. aureus* antibody. Immunostaining counterstained with hematoxylin, × 400. E: Immunohistochemistry for GFAP. Near the ventricle, the GFAP-positive reaction is weakened, possibly because of endotoxin of the bacteria. Immunostaining counterstained with hematoxylin, × 200. F: Immunohistochemistry for Iba-1. Iba-1-positive microglias are diffusely observed in the parenchyma. Immunostaining counterstained with hematoxylin, × 200.

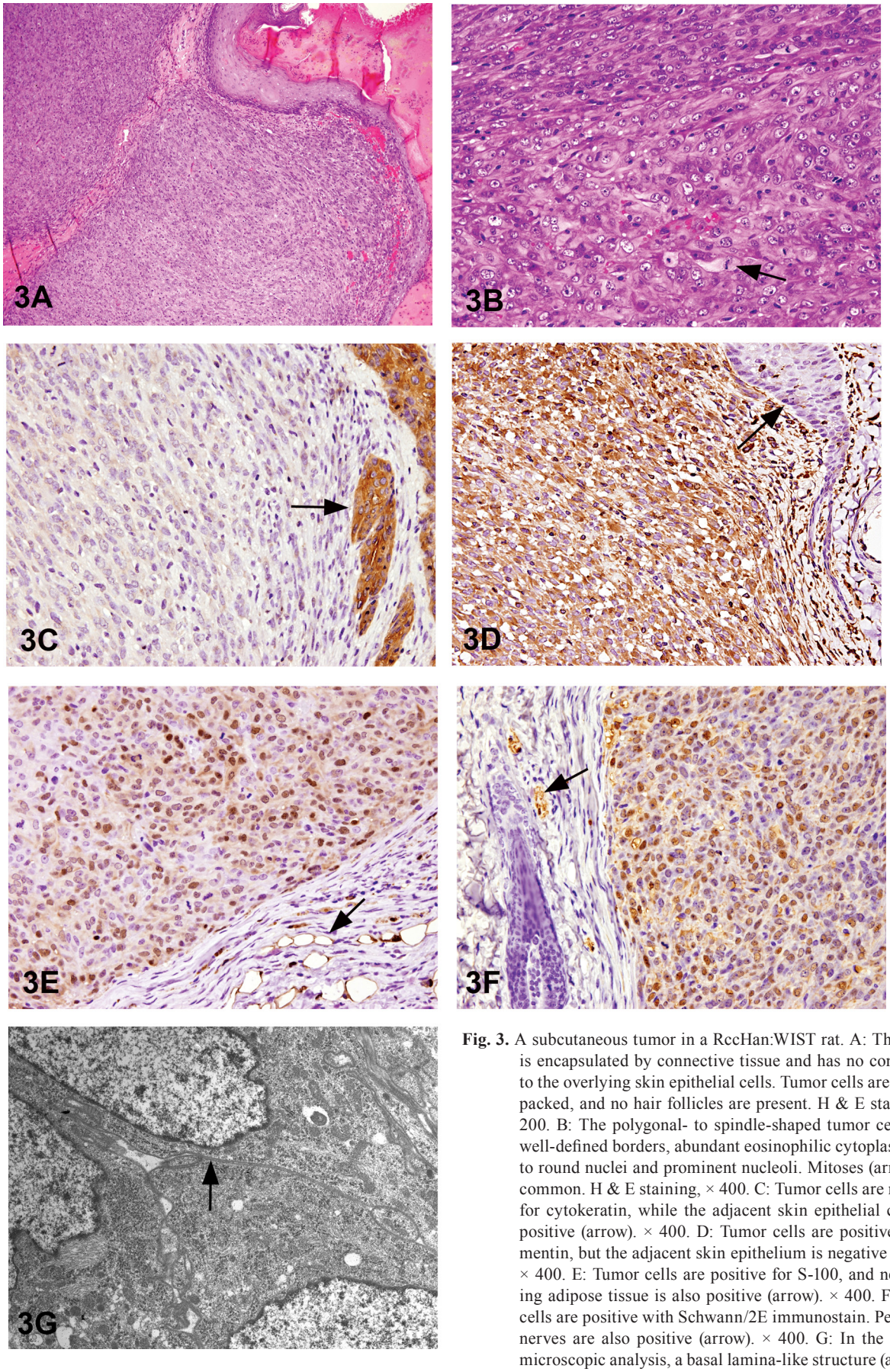

Fig. 3. A subcutaneous tumor in a RccHan:WIST rat. A: The tumor is encapsulated by connective tissue and has no connection to the overlying skin epithelial cells. Tumor cells are densely packed, and no hair follicles are present. H & E staining, × 200. B: The polygonal- to spindle-shaped tumor cells have well-defined borders, abundant eosinophilic cytoplasm, oval to round nuclei and prominent nucleoli. Mitoses (arrow) are common. H & E staining, × 400. C: Tumor cells are negative for cytokeratin, while the adjacent skin epithelial cells are positive (arrow). × 400. D: Tumor cells are positive for vimentin, but the adjacent skin epithelium is negative (arrow). × 400. E: Tumor cells are positive for S-100, and neighboring adipose tissue is also positive (arrow). × 400. F: Tumor cells are positive with Schwann/2E immunostain. Peripheral nerves are also positive (arrow). × 400. G: In the electron microscopic analysis, a basal lamina-like structure (arrow) is present, but no premelanosomes are observed.

Table 2. Summary of Immunohistochemical Results

Antibody (clone)	Results
Cytokeratin (AE1/AE3)	-
S-100	+++
Schwann/peripheral myelin (Schwann/2E)	+++
CD68 (ED-1)	+ (only infiltrative macrophages)

ing, a positive reaction was observed in the peripheral cells that corresponded to the cell border (data not shown). In the electron microscopic analysis, a basal lamina-like structure was observed as a doublet line around the cells, and premelanosome-like round structures were not observed in the cytoplasm (Fig. 3G). Taking these results (basal lamina-like structure, lack of premelanosomes) into consideration, this tumor could be considered a malignant schwannoma. However, this tumor did not show Antoni A or B proliferation patterns and had abundant cytoplasm, suggestive of an epithelial tumor.

In the rodent toxicological pathology literature, there is no report of an "epithelioid" type of schwannoma, but in the medical and veterinary fields, "epithelioid" schwannoma cases have been reported[7–10]. There is a particularly large number of reports in the human literature, and schwannomas have been classified not only as Antoni type A and B but also as plexiform, epithelioid and melanotic types, etc.[7] This case is thought to be classified as an epithelioid type; however, epithelioid Schwann cells are generally observed partially within typical Antoni A or B patterns[7].

Using only the H&E images, this case was considered hard to diagnose. But the voting choices and results were (1) basal cell tumor, benign (7%); (2) basal cell tumor, malignant (27%); (3) melanoma (18%); (4) schwannoma, benign (6%); (5) schwannoma, malignant (26%); (6) squamous cell carcinoma (6%); (7) trichoepithelioma (9%); and (8) other (1%). Contrary to the speaker's expectation, many audience members voted for schwannoma, malignant. One of the discussion points was a question about the origin of this tumor. One audience member suggested "neural crest" cell as a potential origin. However, based on our findings, the tumor origin was not clear, so the recommendation was to not specify the origin.

Nasal Septum Hyalinosis/Eosinophilic Substance

Dr. Hiroaki Nagai (Nihon Nohyaku Co., Ltd., Osaka, Japan) presented a spontaneous lesion in the nasal septum of 2-year-old B6C3F1 mice used in NTP chronic bioassays. At the 2010 NTP Satellite Symposium, this lesion was originally presented by Dr. Elmore (NIEHS and the NTP, Research Triangle Park, NC, USA). At that time, the majority of the audience voted for "nasal septum hyalinosis" (52%), and the second choice was "eosinophilic substance"[3] (21%). In the current JSTP/NTP satellite symposium, the voting results based upon several images (Figs. 4A and B as examples) were nasal septum hyalinosis (32%), eosinophilic substance (22%), interstitial hyalinosis (18%), amyloid (15%), nasal gland proteinosis (10%), nasal gland secretion (3%) and other (0%). The lesion was characterized by the deposition of an amorphous, acellular, and eosinophilic material within the nasal septum at levels I and II, with various degrees of severity. It appeared that the material was associated with the nasal glands and the vomeronasal organ, but inflammation and degeneration were not present. To characterize the material, Congo red staining was performed because morphologically this lesion looks like amyloid, however, the material itself did not produce any birefringence with polarization (Fig. 4C). The material was stained pale blue with Masson's trichrome (Fig. 4D), and silver impregnation revealed that reticulin fibers were sparse within the material and that there was disruption of the nasal gland basement membrane (Fig. 4E). PAS staining with a prior diastase treatment stained the material dark magenta and similar material was seen within the nasal glands (Fig. 4F). In the area with large amounts of interstitial material, there was a smaller volume of material within the nasal glands; therefore, it appeared that the interstitial material had "leaked" from the nasal glands due to disruption of the glandular basement membranes.

Similar lesions were previously diagnosed as an "eosinophilic substance"[11–13]. The material was reported to be Congo red negative, pale blue with Masson's trichrome and dark magenta with PAS. Electron microscopy revealed no non-branching fibers, indicating that this material was not amyloid. Electron microscopy also revealed that this "eosinophilic substance" consisted of amorphous material and collagen. There was occasional disruption of the nasal gland epithelial cell basement membrane where this interstitial material was continuous with the material within the cytoplasm of the epithelial cell and also continuous with the material in the rough endoplasmic reticulum. These findings suggested that the material was produced as a secretion product that leaked into the interstitium through disruption of the basement membranes.

After the presentation, there was discussion about whether or not to rename this lesion as "nasal septum hyalinosis," since it has already been reported in the literature three times as "eosinophilic substance" by Doi *et al.*[11–13] A revote resulted in nasal septum hyalinosis (48%), eosinophilic substance (46%), nasal gland proteinosis (3%), interstitial hyalinosis (2%), nasal gland secretion (2%), amyloid (0%) and others (0%). These voting results indicate that all audience members agreed that this lesion was not amyloid, although this is the diagnosis in the current INHAND document[14]. A consensus was not obtained, so there still needs

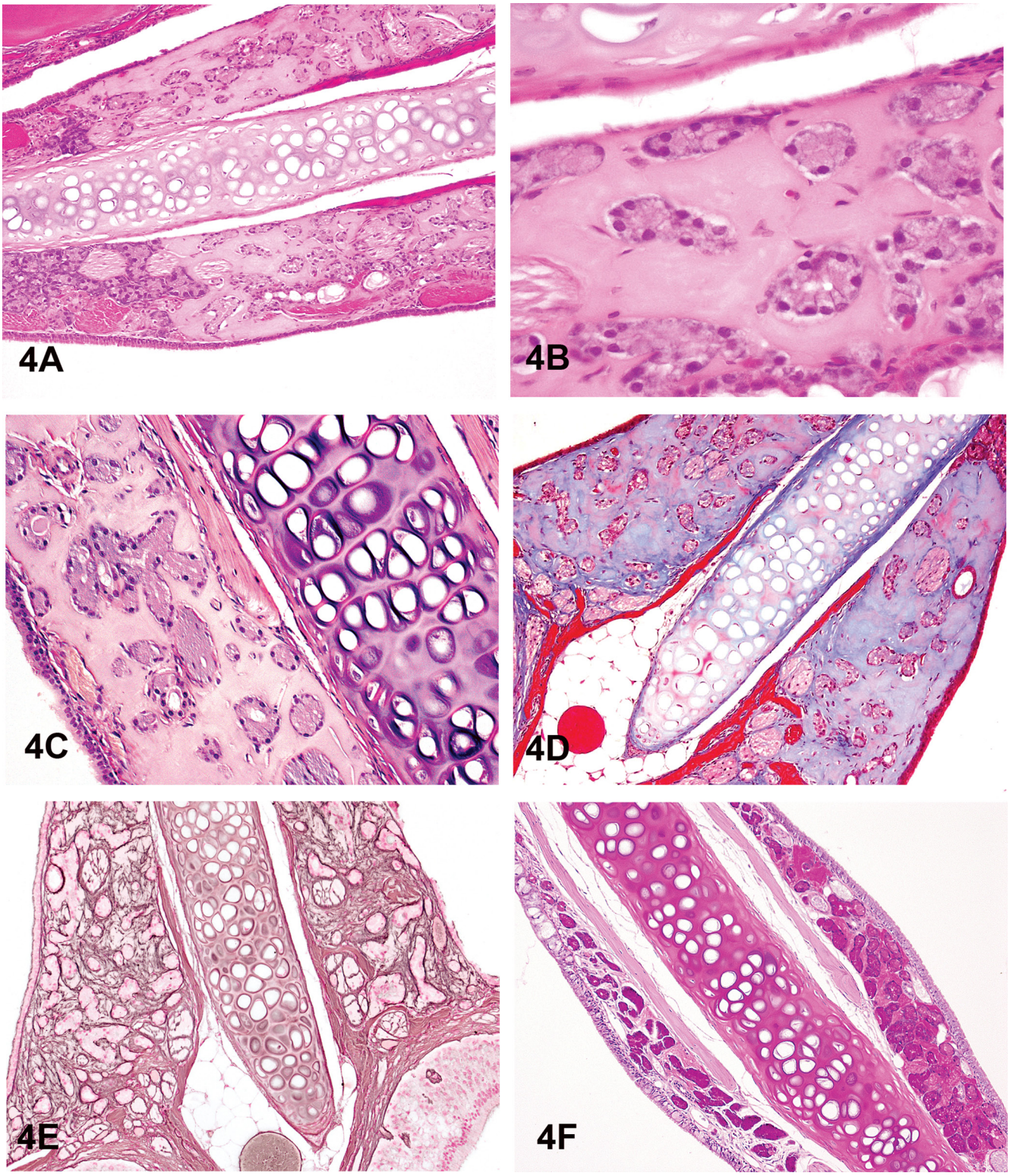

Fig. 4. Non-amyloid eosinophilic material within the nasal septum at levels I and II in 2-year-old B6C3F1 mice. A&B: This lesion is characterized by an amorphous and acellular eosinophilic material within the nasal septum. The material is closely associated with the nasal glands, and there is a lack of inflammation and degeneration. H & E staining. C&D: The material is negative with Congo red (C) and stains pale blue with occasional red areas with Masson's trichrome (D). E: A silver stain reveals that reticulin fibers are sparse within the material and that the glandular basement membrane is partially disrupted around some glands. F: The material stains dark magenta with periodic acid-Schiff (PAS). When the material is within the glands, it is dark magenta (left side of the nasal septum), but when there is leakage into the interstitium, there is less material within the glands, and therefore the staining is not as dark (right side of the nasal septum).

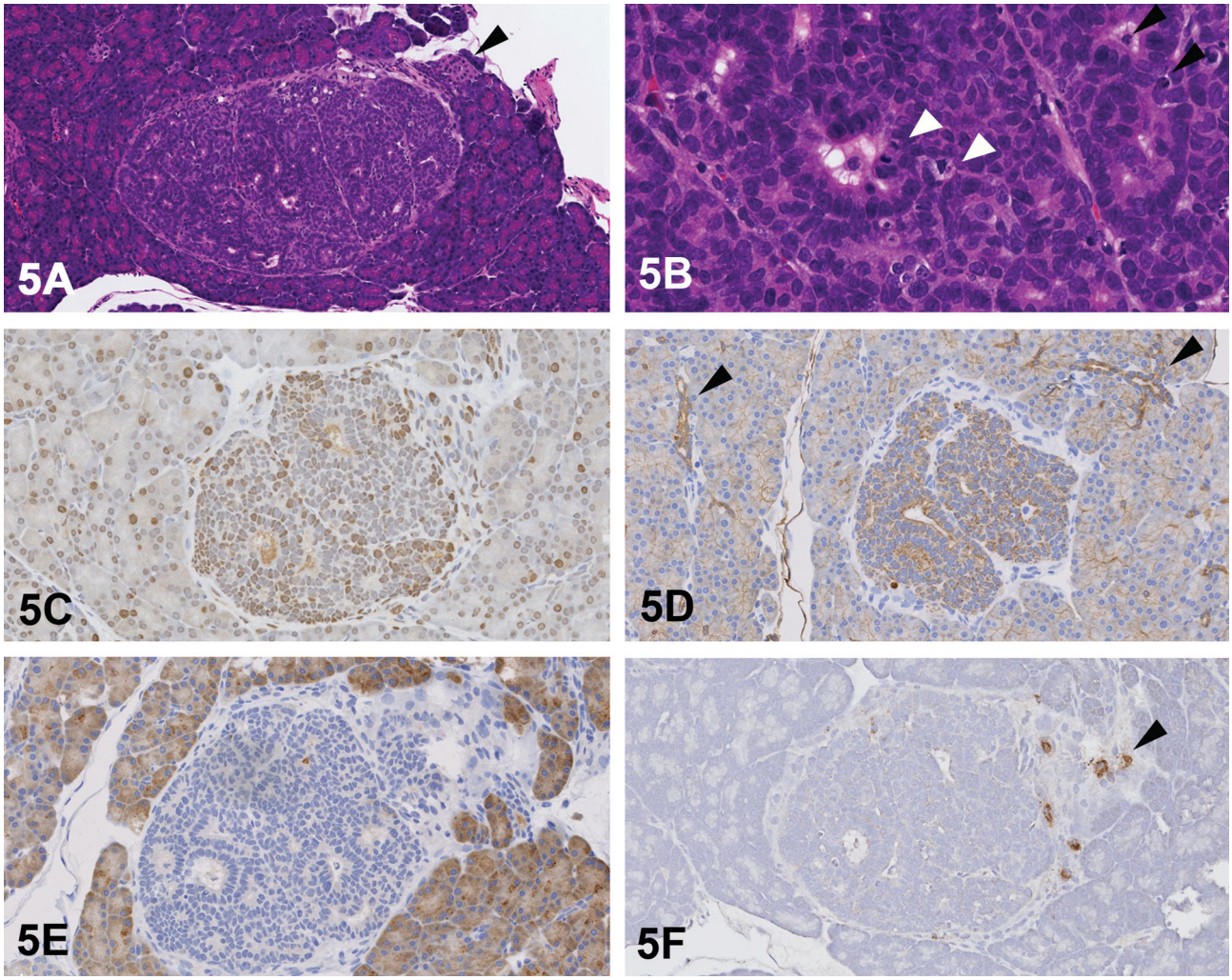

Fig. 5. Pancreatic ductal cell lesion in a 21-day-old female Lewis rat treated with *N*-methyl-*N*-nitrosourea (MNU). A: A solitary pancreatic nodule with encapsulation and slight compression of the surrounding tissue. A focus of normal islet cells is adjacent to the nodule (arrowhead; H & E staining). B: Cells within the nodule from ductular structures composed of cells with larger nuclei and less cytoplasm, without zymogen granules. Note the mitotic figures (white arrowheads) and apoptotic cells (black arrowheads). (H & E staining). C: Proliferating cell nuclear antigen (PCNA) immunohistochemistry showing many positive intralesional cells. Some surrounding acinar cells are also positive for PCNA because their cells seem to have proliferative activity at the age of 21 days. D: Pan-cytokeratin (CK) immunohistochemistry shows that cellular cytoplasm within this nodule is strongly positive for CK, as are the surrounding normal ductal cells (arrowheads). E: Immunohistochemistry using alpha-amylase shows that the cytoplasm of normal acinar cells is strongly positive for amylase; however, no signals are seen within this nodule. F: Immunohistochemistry using an insulin marker shows that no signals are detected in the cytoplasm of cells within this nodule. However, the surrounding normal islet cells are positive (arrowhead).

to be more discussion to determine the best diagnostic term for this lesion.

A Pancreatic Ductal Cell Adenoma

Dr. Katsuhiko Yoshizawa of Kansai Medical University presented an unusual pancreatic lesion from a 21-day-old female Lewis rat that was injected once intraperitoneally at birth with 35 mg/kg *N*-methyl-*N*-nitrosourea (MNU). This lesion was a solitary nodule, approximately 500 × 600 µm in length, with encapsulation and slight compression of the surrounding tissue (Fig. 5A). It was characterized by ductal structures composed of cells with large nuclei and scant cytoplasm, without zymogen granules (Fig. 5B). No necrotic areas or inflammation were present in this nodule. Mitoses and expansion of the lesion, combined with proliferating cell nuclear antigen (PCNA)-positive cells, confirmed the proliferative nature of this lesion (Fig. 5C). Some scattered surrounding acinar cells were also positive for PCNA, indicating that these acinar cells have some normal proliferative activity at the age of 21 days.

To confirm the origin of this nodule, various IHC makers were used: pan-cytokeratin (CK) for pancreatic duct cells, amylase for acinar cells and insulin and pancreatic

and duodenal homeobox 1 (PDX-1) for islet cells. PDX-1 is a transcription factor necessary for β-cell maturation and is expressed in the normal islet cells of adult rats[15]. The results of the IHC showed that the cytoplasm of cells within this nodule was more positive for CK than the surrounding normal ductal cells (Fig. 5D). The IHC for alpha-amylase revealed that no signal was seen in the cytoplasm of cells within this nodule (Fig. 5E). The cytoplasm of normal acinar cells was strongly positive for amylase. Immunohistochemistry for insulin (Fig. 5F) and PDX-1 revealed no signals in the cytoplasm of cells within this nodule. However, as an internal positive control, islet cells were positive for insulin and PDX-1. Based on the results of these IHC analyses, the immunoreactivity in this nodule was considered similar to ductal cells, suggesting the origin was "ductal cell."

After viewing only the H&E images, the voting choices and results for this lesion were islet cell hyperplasia (6%), islet cell adenoma (7%), acinar cell hyperplasia (14%), acinar cell adenoma (29%), ductal cell hyperplasia (11%), ductal cell adenoma (29%), and regeneration (2%). In the JSTP/NTP symposium, 43% felt that it was of acinar cell origin and 40% felt that it was of ductal cell origin. This case was also presented at the 2012 NTP Satellite Symposium in Boston[1], and the voting result was similar to the JSTP/NTP Symposium; the results were islet cell hyperplasia (2%), islet cell adenoma (13%), acinar cell hyperplasia (14%), acinar cell adenoma (28%), ductal cell hyperplasia (10%), ductal cell adenoma (32%), and regeneration (1%). The discussion points were whether this lesion is nonneoplastic or neoplastic, and whether this lesion is of islet, acinus, or ductal origin. This lesion was an encapsulated nodule with proliferative activity and showed compression of the surrounding tissue without invasion and cellular atypia. After presentation of the results of the IHC analyses and from the criteria for proliferative lesions of pancreatic ducts[16–18], most audience members agreed that this nodule was a benign ductal adenoma. Some audience members felt that this lesion may be at a stage of regeneration; however, this seemed unlikely because this nodule showed growth and expansion into the surrounding tissue and there was no inflammation or necrosis to indicate prior injury[19].

Eosinophilic Crystalline Pneumonia in a Transgenic Mouse Model

Dr. Mark Hoenerhoff (NTP and NIEHS, RTP, NC, USA) was the sixth speaker of the day and presented an interesting lung lesion found in a colony of transgenic mice. Male and female mice on a C57BL/6 background presented clinically with poor weight gain, weight loss, hunched posture, ruffled hair coat, and tachypnea. Transgenic mice were noticeably smaller than their age- and sex-matched wildtype (WT) littermates. Grossly, lungs of transgenic mice failed to collapse upon opening the thorax, and were diffusely firm, consolidated and mottled dark red to tan (Fig. 6A). Histologically, lungs were characterized by a marked multifocal to coalescing cellular infiltrate composed of large epithelioid macrophages and scattered multinucleate giant cells containing fine, acicular intracytoplasmic eosinophilic crystalline material within alveoli, bronchioles and bronchi (Figs. 6B and C). There were variable perivascular and peribronchiolar inflammatory infiltrates composed predominantly of lymphocytes and plasma cells. Bronchiolar epithelial hyperplasia was also present. In more severely affected regions of the lung, there was multifocal thickening of alveolar septa with type II pneumocyte hyperplasia, and interstitial and perivascular fibrosis (Fig. 6D). Voting choices and responses were 1) granulomatous pneumonia (2%), 2) acidophilic macrophage pneumonia (44%), 3) histiocytic pneumonia (16%), 4) eosinophilic crystalline pneumonia (20%), 5) alveolar proteinosis (13%), 6) crystalline pneumonitis (1%), 7) histiocytic infiltrate (2%), and 8) other (1%). A majority of conference participants (44%) preferred the term acidophilic macrophage pneumonia, whereas the presenter indicated that eosinophilic crystalline pneumonia (ECP), chosen by 20% of the audience, is the preferred term for this lesion. The membership of the STP at the 2012 NTP Satellite Symposium chose ECP (53%) as the preferred term, whereas 31% chose acidophilic macrophage pneumonia. Other voting choices ranged from 0–6%[1].

While acidophilic macrophage pneumonia and crystalline pneumonitis are diagnoses also used to describe this lesion, this nomenclature is outdated and not currently used

Fig. 6. Eosinophilic crystalline pneumonia in a transgenic mouse model. A: Gross photomicrograph of lungs from a transgenic mouse (right) and age- and sex-matched wildtype littermate. Lungs from the transgenic mouse are diffusely consolidated, fail to collapse, and are mottled red to tan. B: Transgenic mouse lung. Low power photomicrograph demonstrating the coalescing to diffuse and fulminant nature of the cellular infiltrate; approximately 90% of the lung is invested with a dense cellular infiltrate within alveolar spaces and airways. C: Transgenic mouse lung. High-power photomicrograph illustrating the cellular infiltrate composed of large epithelioid macrophages and occasional multinucleate giant cells (inset) containing fine intracytoplasmic eosinophilic crystalline material and rare needle-shaped extracellular crystals (arrow). D: Transgenic mouse lung. Severely affected regions of lung demonstrate multifocal alveolar wall thickening (white arrows) with fibrosis and type II pneumocyte hyperplasia, and perivascular and peribronchiolar (black arrows) fibrosis. E: Immunohistochemistry for CHI3L3 protein, transgenic mouse lung. Macrophages, multinucleate cells and crystalline material are immunoreactive for CHI3L3 protein (anti-CHI3L3 antibody, hematoxylin counterstain). F: Luna histochemical stain, transgenic mouse lung. Crystalline material within macrophages and multinucleate cells stains diffusely reddish orange with Luna stain. G: Transmission electron microscopy, transgenic mouse lung. Alveolar macrophages are distended with electron-dense, angular to rectangular, needle-shaped crystalloid inclusions that lack a periodic structure, are composed of dense granular material, and are membrane bound (inset). H: Transmission electron microscopy, transgenic mouse liver. Electron-dense crystalloid inclusions are present within the cytoplasm of Kupffer cells (arrows) in the liver of transgenic mice.

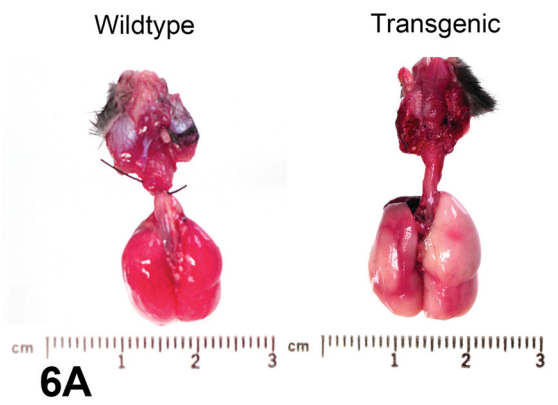
Wildtype
Transgenic
cm
1
2
3
cm
1
2
3
6A

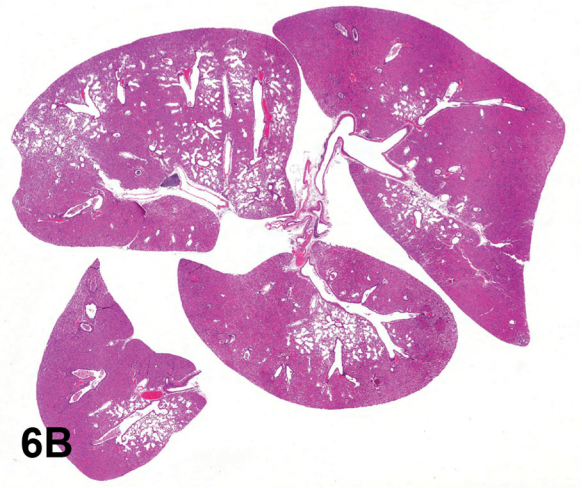
6B

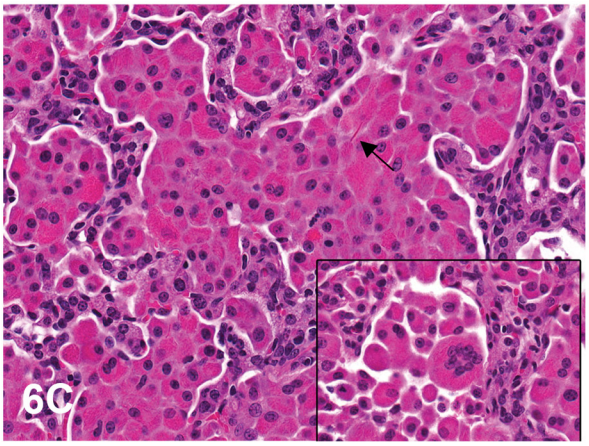
6C

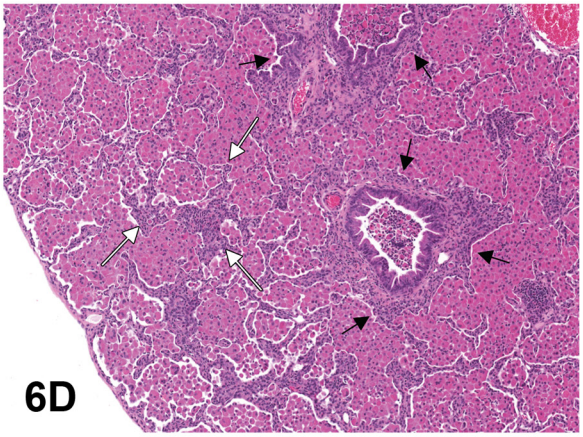
6D

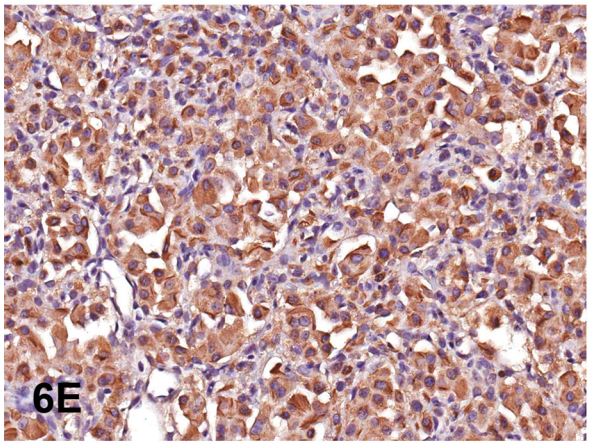
6E

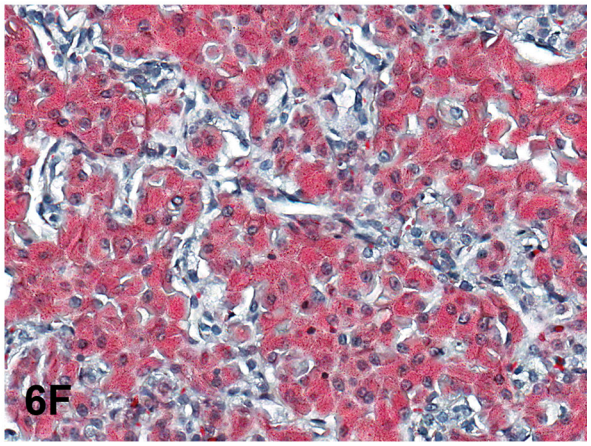
6F

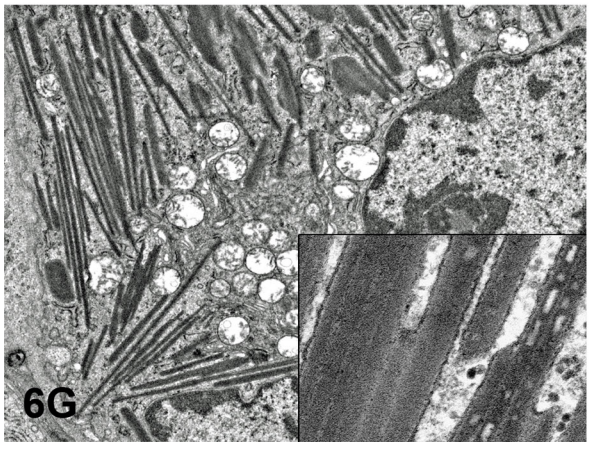
6G

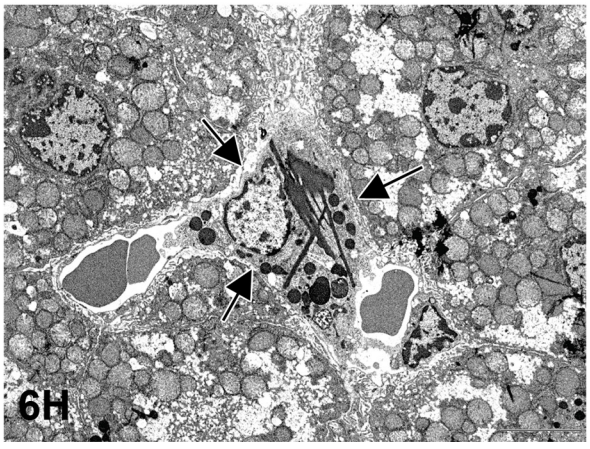
6H

in the scientific literature, and they are thus not the most appropriate diagnoses. While the diagnoses of granulomatous or histiocytic pneumonia were also considered technically correct, they are not considered the most accurate or descriptive terms for the characteristic eosinophilic epithelioid macrophages and multinucleate giant cells containing crystalline material in these lesions. Histiocytic infiltrate was not considered correct since this finding is characterized by a generally mild influx of histologically normal histiocytes within alveoli, rather than the characteristic macrophages and multinucleate cells in this lesion. Alveolar proteinosis is characterized by the presence of eosinophilic proteinaceous fluid within alveolar spaces, and is therefore not an accurate diagnosis for this lesion.

Eosinophilic crystalline pneumonia is a spontaneous idiopathic lesion in mice that varies in incidence and severity depending on a number of host factors, including strain, age, genotype and immune status. The lesion can be mild and asymptomatic to fulminating and fatal. The severity and incidence increases with age in susceptible strains. While this lesion can occur spontaneously, it is also associated with other infectious, inflammatory, and neoplastic pulmonary diseases[20]. This lesion is often seen adjacent to pulmonary adenomas and carcinomas[21]. It is common in models of allergic airway disease, including asthma[22, 23], as well as in inhalation studies such as those for kaolin and tobacco smoke[24, 25]. It is associated with certain infectious diseases, most notably fungal and parasitic respiratory infections including pneumocystosis, cryptococcosis and nematodiasis[21, 26–28]. Background strain plays a significant role in the susceptibility of mice to this disease. It is most common in C57BL/6, 129, B6;129 strains and their derivatives[20, 21, 29] and is a major cause of fatality in aging 129S4/SvJae mice, accounting for 50% of deaths by 24 months of age in this strain[30, 31]. Besides background strain, alterations in genotype can influence the incidence of this lesion, particularly in models of immune dysfunction such as *Cyp1a2*$^{-/-}$, p47$^{phox-/-}$ and Gp91$^{phox-/-}$ mice[29, 32, 33], and immunocompromised strains including the *Ptpn6*^{mo} (motheaten) mouse[34, 35], which is deficient in B, T, and natural killer (NK) cells, the athymic nude mouse, which is deficient in functional T cells, and the severe combined immunodeficient mouse (SCID), which is deficient in B and T cells[21].

Studies investigating eosinophilic crystalline pneumonia have shown that macrophages and intracellular and extracellular crystals are composed of a chitinase-like protein, Chitinase 3-like 3 (CHI3L3) protein, which lacks normal chitinase enzymatic activity[36]. Macrophages, multinucleate giant cells and crystalline material were immunoreactive to CHI3L3 in this series of transgenic mice (Fig. 6E). This protein is normally expressed at low levels in pulmonary and splenic macrophages and bone marrow myeloid progenitors and appears to be induced by a variety of inflammatory, chemical, or physical stimuli[37]. While the exact function of CHI3L3 is still poorly understood, it may have a role in host defense since, as a chitinase-like protein, it retains the ability to bind fungal or parasitic pathogens containing chitin[21], and as such, it also stains reddish orange with a Luna histochemical stain, which is known to bind to chitin (Fig. 6F). It is upregulated in various allergic or inflammatory diseases, and is mildly chemotactic for eosinophils and promotes a TH2 cytokine response[36, 38]. It may play a role in cell-cell and cell-matrix interactions and possibly extracellular matrix remodeling and tissue repair, since it has the ability to bind polysaccharides and glycosaminoglycans[37, 39]. Finally, since it is expressed in fetal/neonatal liver and adult spleen and bone marrow myeloid cells, it is thought that CHI3L3 may play a role in hematopoiesis[40].

Ultrastructurally, macrophages were distended with slender, needle-shaped, electron-dense inclusions and were in various stages of degeneration (Fig. 6G). Crystalline inclusions lacked a periodic structure, were composed of granular material and were membrane bound, indicating that these structures were not in fact true crystals, but rather crystalloid inclusions (Fig. 6G, inset). Since they were membrane bound, they were most likely contained within organelles such as endoplasmic reticulum, lysosomes or mitochondria. Some investigators have demonstrated CHI3L3 in rough endoplasmic reticulum[37], while a similar membrane-bound material has also been shown to accumulate in degenerating mitochondria as a result of mitochondrial dysfunction and hypoxia[41–43]. Although these crystalloid arrays often appeared to be associated with degenerating mitochondria, the definitive origin of this material is difficult to determine in this case due to the severity of the lesions. Regardless, the accumulation of this material appears to represent a general dysfunction in the metabolism of these alveolar macrophages.

Crystalloid arrays were not exclusively found in macrophages within the lung. In the liver, similar inclusions were observed in Kupffer cells lining sinusoids by electron microscopy (Fig. 6H). Therefore, this may be indicative of a systemic or general antigen-presenting cell defect. Alternatively, if CHI3L3 protein in the lung entered the vasculature and was phagocytosed by Kupffer cells in the liver, this would account for the presence of this material in these cells. Further studies are required to determine the origin of this material and chronology of this lesion.

In conclusion, eosinophilic crystalline pneumonia is an idiopathic lesion in mice that is influenced by host factors such as strain, age, genotype and concurrent disease. It is associated with aberrant expression of CHI3L3 protein, in this case likely a result of macrophage dysfunction due to aberrant expression of the transgene. This is a unique lesion in the mouse and a fairly common finding in certain strains. It is therefore critical for the pathologist to have an awareness and understanding of strain-related pathology and background lesions in order to understand the relevance of a particular lesion or strain-related phenotypes.

Hyaline Glomerulopathy in ddY Mice

Dr. Tomoaki Tochitani (Dainippon Sumitomo Pharma Co., Ltd., Osaka, Japan) presented glomerular lesions in two

female ddY mice that were characterized by diffuse, global deposition of amorphous eosinophilic material. The images presented for voting were from kidney sections stained with H&E, Congo red, Masson's trichrome, periodic acid–Schiff (PAS), and periodic acid methenamine silver (PAM) stains (Figs. 7A–D).

The voting choices and results were amyloidosis (2%), hyaline glomerulopathy (65%), collagenofibrotic glomerulonephropathy (18%), glomerulosclerosis (8%), membranous glomerulopathy (7%) and "other" (0%). It is usually difficult to differentiate hyaline glomerulopathy from amyloidosis in H&E sections because of the morphological similarity between these two entities. However, maybe because the results of the special stains were shown before voting, the majority of the participants voted for hyaline glomerulopathy, in concurrence with speaker's diagnosis. Also, the difference between hyaline glomerulopathy and amyloidosis might now be well recognized because "eosinophilic glomerular deposits" were recently addressed at the 2010 NTP Satellite Symposium [3].

Animals were purchased for microbial monitoring at four weeks of age and were kept untreated until necropsy at fourteen weeks of age. These animals had renal lesions characterized by diffuse, global deposition of amorphous eosinophilic material within the glomeruli (Figs. 7A and B). The glomerular deposits were negative for Congo red with polarized light (Fig. 7C) but positive for PAS. In addition, the deposits were stained red with Masson's trichrome (Fig. 7D). Deposits were negative for PAM, and the basement membrane was not thickened. Immunohistochemically, the deposits were positive for IgG, IgM, IgA and C3 (data not shown). Electron microscopically, the deposits consisted of microtubular structures with diameters of 80–100 nm and fibrillar structures with diameters of 9–16 nm (Figs. 7E and F). Based on these characteristics, these glomerular lesions were diagnosed as hyaline glomerulopathy.

Hyaline glomerulopathy was first diagnosed in aging B6C3F1 mice and is generally known as a spontaneous lesion in aging mice[44]. Also, induced cases of hyaline glomerulopathy have been reported in pulegone-treated rats and mice[3, 45]. Glomerulonephritis, characterized by similar prominent hyalinization of glomeruli, was also reported as a spontaneous lesion in a female rasH2 mouse[46]. In these cases, eosinophilic deposits were positive for PAS and immunoglobulins and characterized by subendothelial osmiophilic deposits composed of fibrillary structures with diameters of 7–14 nm[3, 44, 46].

The deposits in the ddY mice consisted of microtubular structures with diameters of 80–100 nm and fibrillary structures with diameters of 9–16 nm. Light and ultramicroscopic findings of the glomeruli in the two ddY mice were similar to those of immunotactoid glomerulopathy or fibrillary glomerulonephritis in humans[47–50], although these entities have not been defined in rodents. Immunotactoid glomerulopathy and fibrillary glomerulonephritis are characterized by glomerular deposits that are negative for Congo red and positive for immunoglobulins such as IgG, IgM, IgA and C3. The glomerular deposits of fibrillary glomerulonephritis are observed in electron microscopy as electron-dense deposits that are nonbranching fibrillary structures, similar in appearance but larger than amyloid fibrils[48–50]. Immunotactoid glomerulopathy is defined by glomerular deposition of immunoglobulin with a substructural organization of hollow, stacked microtubules of ≥30 nm, whereas fibrillary glomerulonephritis is defined by deposition of randomly oriented fibrils of <30 nm in diameter[47–50].

Hyaline glomerulopathy is now used as a term to describe glomerular lesions characterized by the deposition of non-amyloid amorphous eosinophilic materials in the H&E section, and there are also some differences in immunohistochemical or ultrastructural features in these reports. So it is important to note that this term does not define the interglomerular material. One audience member noted how the glomerular lesions in pulegone-treated mice versus ddY mice look the same by light microscopy and PAS staining and are both called hyaline glomerulopathy. But while the lesion in ddY mice contains predominately immunoglobulins and stains red with Masson's trichrome, the interglomerular material in pulegone-treated mice contains trapped immunoglobulins and stains blue with Masson's trichrome, and the identity of the bulk of the material is as yet unknown. A good take home point is that not all hyaline glomerulopathies are the same, and emphasis should be placed on the prominent role of electron microscopy in differentiation of immune complex deposits from other organized deposits.

Intrahepatocytic Erythrocytes and Subendothelial Hepatocytes in B6C3F1 Mice

Dr. Elmore (NTP and NIEHS, Research Triangle Park, NC, USA), in collaboration with Drs. Jim Morrison and Linda Kooistra (Charles Rivers Laboratories, Pathology Associates, Durham, NC, USA), presented two unusual liver lesions in mice. The first case was from female B6C3F1 mice in a 28-day NTP immunotoxicity study. The route of administration was oral gavage. After showing a series of images (Figs. 8A and B), the audience was asked to vote. The voting choices and results were 1) artifact (8%), 2) angiectasis (0%), 3) emperipolesis (5%), 4) erythrophagocytosis (32%), 5) intrahepatocytic erythrocytes (22%), 6) hepatic erythrophagocytosis (26%), 7) hepatocyte cytoplasmic inclusions (7%) and 8) other (0%). The three top choices were similar to the 2012 NTP Satellite Symposium votes[1]: erythrophagocytosis (25%), intrahepatic erythrocytes (33%) and hepatic erythrophagocytosis (33%).

Dr. Elmore then discussed some important diagnostic features. This lesion generally occurs in groups of enlarged hepatocytes containing one to many red blood cells (RBCs) within the cytoplasm. The hepatocyte nucleus may be centrally located with slightly condensed chromatin. If there are many RBCs, the nucleus may be pushed peripherally. The cytoplasm of adjacent hepatocytes is often of decreased density. Transmission electron micrographs showed that the RBCs did not appear to be confined by a lysosomal mem-

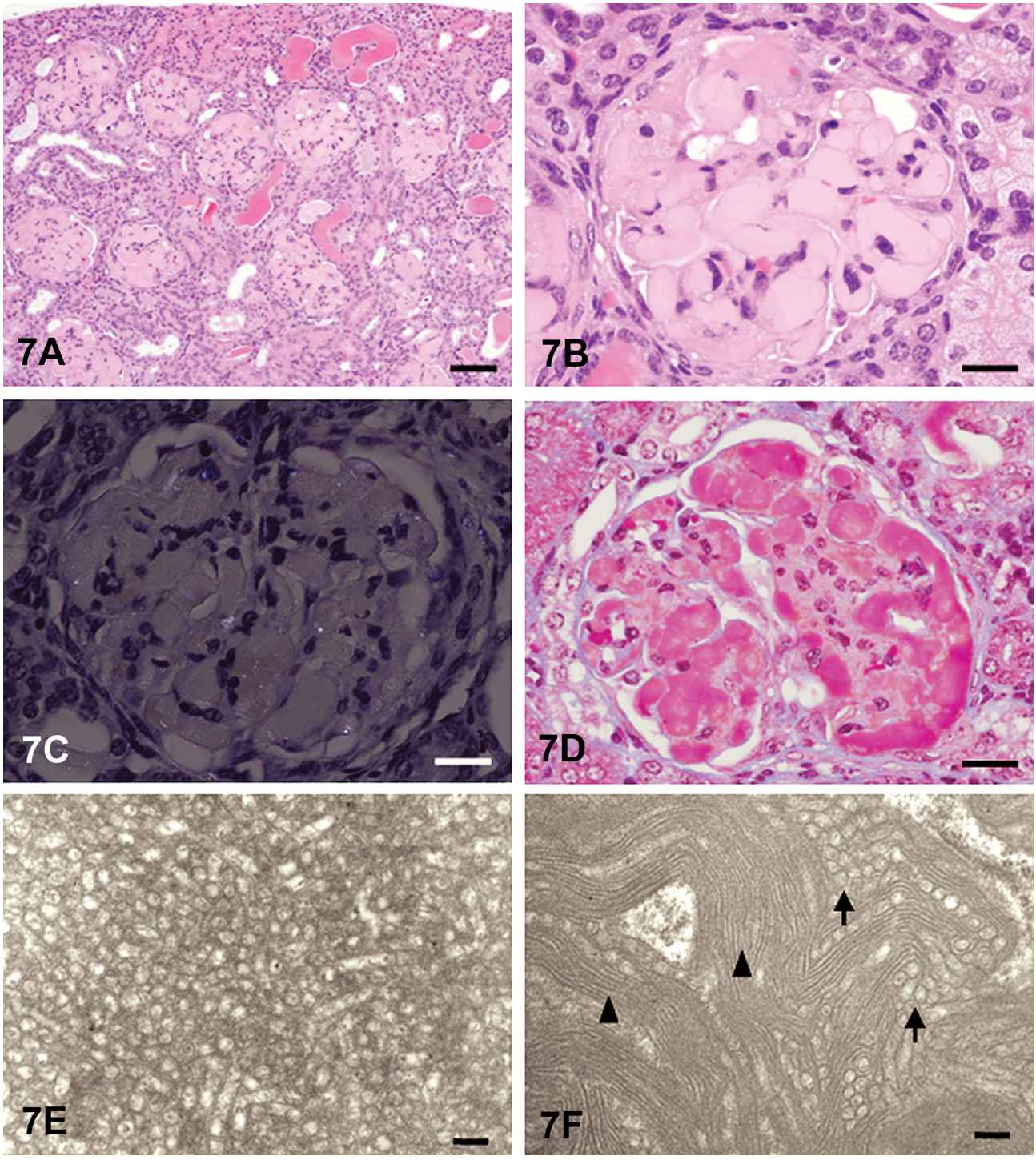

Fig. 7. Hyaline glomerulopathy in ddY mice. A: The glomeruli are enlarged due to deposition of amorphous eosinophilic material. H & E staining, bar=200 mm. B: Higher magnification of an enlarged glomerulus with deposition of eosinophilic material. Collapse of capillary lumens and expansion of the mesangial region are observed. H & E staining, bar=50 mm. C: The glomerular deposits are negatively stained with Congo red, and there is no green birefringence with polarized light. Congo red with polarized light, bar=50 mm. D: The glomerular deposits are stained red with Masson's trichrome. Masson's trichrome, bar=50 mm. E: Electron microscopy shows microtubular structures with diameters of approximately 80–100 nm and hollow centers. Bar=200 nm. F: Electron microscopy shows microtubular (arrows) and fibrillary (arrowheads) structures with diameters of 80–100 and 9–16 nm, respectively. Bar=200 nm.

brane (Figs. 8C and D). This finding eliminated both macrophage and hepatocyte-mediated erythrophagocytosis as potential diagnoses. The RBCs were also clearly within the cytoplasm of the hepatocyte and not within the endothelial lined spaces, eliminating angiectasis as a potential diagnosis. Emperipolesis is the active penetration of one intact cell

by another cell with both cells remaining viable. This differs from phagocytosis in that the cells enter another cell by an active process, remain viable, and can exit again with no damage to either cell. Hepatocyte cytoplasmic inclusions is another potential differential; however this terminology does not indicate that RBCs are the inclusions.

After consideration of the histology and electron microscopy findings, the NTP decided that, for their studies, "intrahepatocytic erythrocytes" (i.e., intrahepatocellular erythrocytes) would be the most appropriate diagnosis. This lesion is treatment related in many NTP studies, although a few cases have been seen in controls. It has been seen in both male and female rats and mice and in both short- and long-term studies[1]. However, the pathogenesis and significance of this lesion remains unknown.

Dr. Elmore's next presentation was another unusual liver lesion in female B6C3F1 mice from a 2-year pulegone gavage carcinogenicity bioassay. After reviewing a series of images (Figs. 8E–H), the audience was given diagnostic choices and asked to vote. The voting choices and results were 1) vascular pseudoinvasion (5%), 2) intravascular hepatocytes (31%), 3) venous intramural hepatocytes (22%), 4) vascular infiltration of hepatocytes (9%), 5) subendothelial hepatocytes (26%), 6) metastatic hepatocellular carcinoma (1%), and 7) extension of perivascular focus of cellular alteration (6%). The majority of audience members voted similar to the 2012 NTP Satellite Symposium participants, who chose intravascular hepatocytes (17%), venous intramural hepatocytes (23%), or subendothelial hepatocytes (50%) as their top three choices[1].

Pulegone is a naturally occurring organic compound obtained from the essential oils of a variety of plants such as peppermint, pennyroyal and *Nepeta cataria* (catnip). It has a minty taste and is used in flavoring agents, perfumery and aromatherapy. This lesion was found as a treatment-related lesion in the NTP chronic bioassay for pulegone, which used 50 animals per group, in males (control-3, low dose-1, mid dose-15, high dose-47) and females (control-0, low dose-2, mid dose-20, high dose-46).

This lesion is infrequently seen in control and treated mice. The pathogenesis and biological significance are unknown. The lesion in this study usually involved medium- and large-size hepatic veins. Dr. Elmore presented images of immunohistochemistry and special stains to further characterize this lesion. CD31 (i.e. PECAM-1) is a membrane protein that mediates cell-to-cell adhesion and is made in endothelial cells. Factor-III-related antigen (i.e., von Willebrand factor) is made and stored in endothelial cells. Both of these immunostains showed that the infiltrating hepatocytes were covered by an endothelial lining (Figs. 8I and J). Trichrome, which detects collagen, highlighted the vascular wall and also showed some faint collagen remodeling of the luminal lining of the hepatocytes (Fig. 8K). This stain also showed hepatocytes migrating through the vein wall (Fig. 8L). Smooth muscle actin highlighted the original vascular wall (data not shown). Together, these stains showed that the hepatocytes infiltrated the vein wall, protruded into the vein lumen and were covered by an endothelial lining. Audience discussion suggested that this most likely occurred by re-endothelialization.

This lesion has not been recorded in previous NTP studies. However, it has been reported in diethylnitrosamine-treated mice. A previous report in diethylnitrosamine- treated mice noted this lesion within basophilic foci, with extension into a central vein[51,52]. In the present case, the subendothelial hepatocytes were not associated with basophilic foci. This lesion has also been published in the *International Harmonization of Nomenclature and Diagnostic Criteria (INHAND): Proliferative and Nonproliferative Lesions of the Rat and Mouse Hepatobiliary System* guidelines[53]. In this document, it is described as a protrusion of normal-appearing hepatocytes into hepatic veins and within the contour of the vessel, usually involving medium- to large-size hepatic veins. However, the INHAND document suggests that this lesion be diagnosed as "intravascular hepatocytes." Since the infiltrating hepatocytes are covered by an endothelial lining, "subendothelial hepatocytes" may be considered a more appropriate diagnostic term.

In summary, the important findings of this lesion are 1) it usually involves medium- to large-size hepatic veins, 2) hepatocytes protrude into the vein lumen and infiltrate the vein wall, 3) infiltrating hepatocytes are covered by an endothelial cell lining, 4) it is rarely seen in control or treated mice, and 5) it is not necessarily within basophilic foci or associated with other hepatic lesions. The significance and pathogenesis of this lesion remain unknown.

Vacuolar Degeneration of Thyroid Follicular Cells in a Cynomolgus Monkey

Dr. Hiroshi Satoh (FUJIFILM Corporation, Minamiashigara, Kanagawa) was the ninth speaker of the day and presented a spontaneous thyroid lesion in a cynomolgus monkey. The project was conducted in collaboration with Drs. Hirofumi Hatakeyama, Haruko Koizumi, and Akihito Shimoi (Ina Research Inc., Ina, Nagano). This thyroid follicular cell lesion was observed in an untreated female cynomolgus monkey assigned to a control group. After reviewing low- and high-magnification images and a Periodic acid-Schiff image of the lesion, the audience was asked to vote. The diagnostic voting choices for the case were (1) vacuolar degeneration of the follicular cell, (2) vacuolar degeneration of the C-cell, (3) follicular cell hypertrophy, (4) C-cell hypertrophy, (5) follicular cell hyperplasia, (6) C-cell hyperplasia, (7) follicular cell adenoma, and (8) C-cell adenoma. The votes of the audience participants were divided into approximately half; vacuolar degeneration of the follicular cell (47%) and follicular cell hypertrophy (47%) received the majority of votes, with fewer votes for follicular cell hyperplasia (4%), vacuolar degeneration of the C-cell (1%), C-cell hypertrophy (1%) and follicular cell adenoma (1%).

After the vote, Dr. Satoh showed several images of the thyroid lesion, including a transmission electron mi-

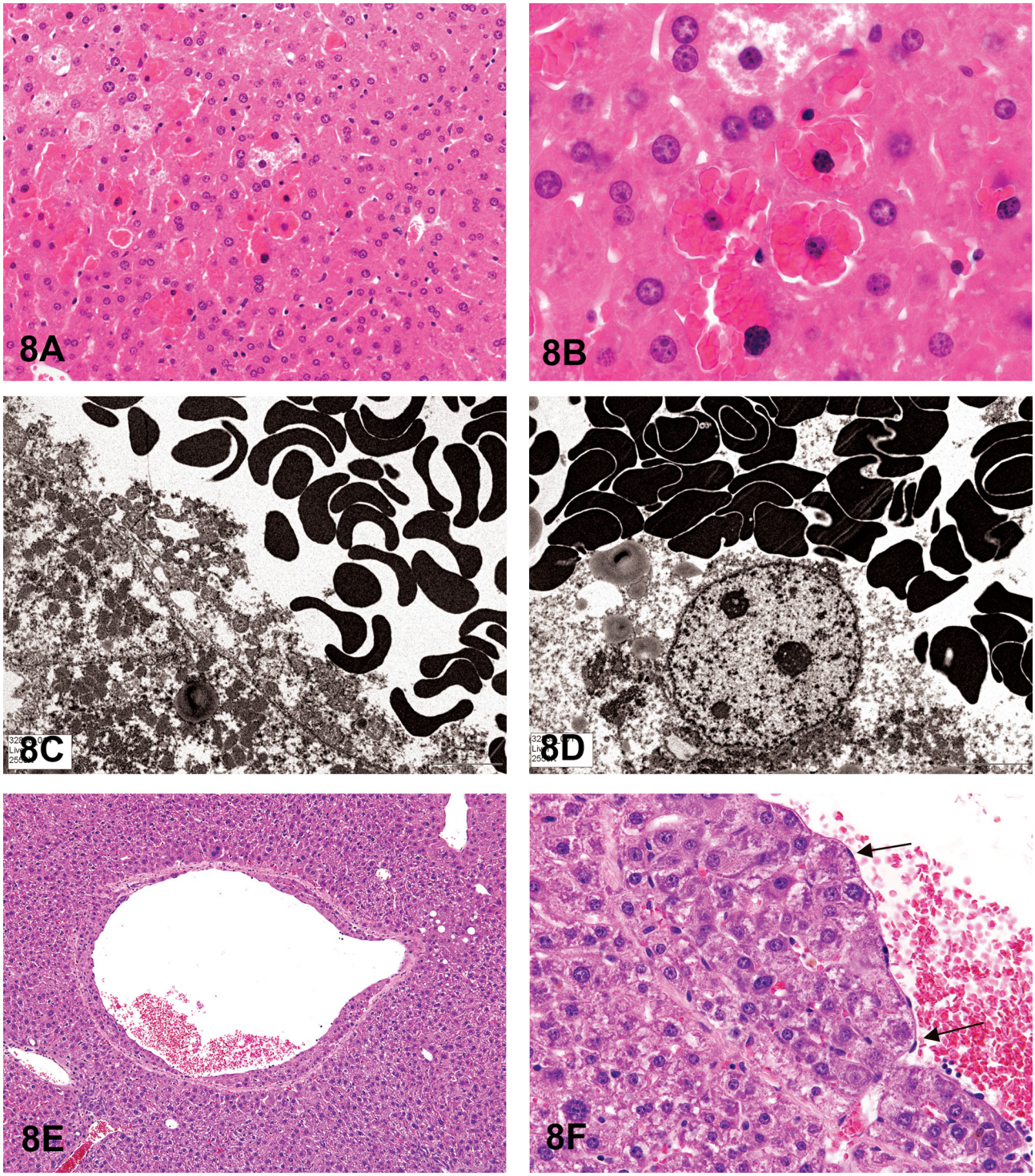

Fig. 8A–D. Intrahepatocytic erythrocytes in female B6C3F1 mice in a 28-day immunotoxicity study. A: Multifocally, there are intrahepatocellular erythrocytes. The hepatic nuclei are slightly condensed and hyperchromatic and can be either centrally or peripherally located. The adjacent hepatocytes are not affected. H & E staining. B: The affected hepatocytes are still viable. The intracytoplasmic red blood cells appear normal, and there is no hemosiderin pigment. Adjacent hepatocytes may sometimes have a decreased cytoplasmic density. H & E staining. C: Transmission electron microscopy illustrates numerous viable erythrocytes within the hepatocellular cytoplasm. D: Transmission electron microscopy shows that the erythrocytes are not contained within endothelial lined spaces or a lysosomal membrane.

Fig. 8E–L. Subendothelial hepatocytes in pulegone-treated B6C3F1 mice. E: Low magnification image illustrating normal-appearing hepatocytes that have breached the vascular wall of a central vein. H & E staining. F&G: Higher magnifications showing the hepatocytes protruding into the lumen, but with an endothelial lining on the lumen side of the hepatocytes (arrows). H & E staining. H: High magnification image of CD31 expression in the endothelial cells overlying the hepatocytes that are within the vessel wall (arrows). I: Factor VIII-related antigen expression in the endothelial cells overlying the hepatocytes within the vessel wall (arrows). J: Smooth muscle actin immunohistochemical staining of the fibromuscular portions of the hepatic vein wall (arrow). K: Trichrome staining of the wall of central vein that contains subendothelial hepatocytes. This highlights the collagen component of the vascular wall. L: Higher magnification of a trichrome-stained vascular wall showing the invasion through, and partial disruption of, the vessel wall (arrows).

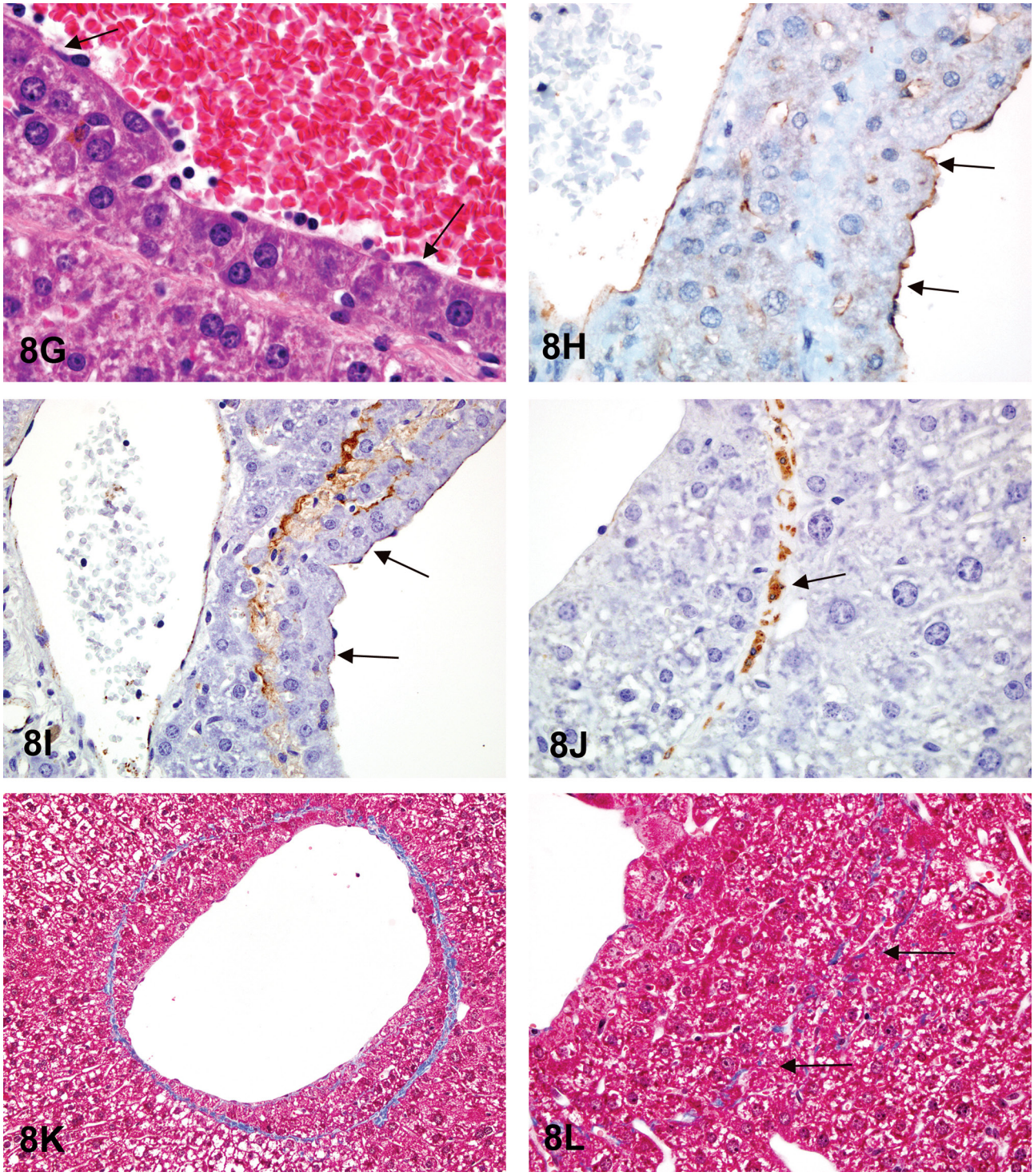

crograph, in order to illustrate why follicular cell vacuolar degeneration was the correct diagnosis. In light microscopy, large vacuoles containing a homogenous substance occupied the basal region of the epithelium, and the nuclei had shifted toward the apical region (Fig. 9A). The vacuoles showed negative reactions with both PAS and anti-thyroglobulin immunohistochemistry (Figs. 9B and C). Electron microscopic observation revealed dilatation of the rough endoplasmic reticulum (RER) corresponding to the vacuoles (Fig. 9D).

Similar lesions, including the present case in cynomolgus monkeys, have previously been diagnosed and reported as vacuolar degeneration of the follicular epithelium[54]. Vacuolar degeneration refers to a large central vacuole or several vacuoles that displace the nucleus peripherally and is most frequently due to the accumulation of hydropic substances in the cytoplasm. Vacuolated cells are generally hypertrophic due to the abnormal accumulation of hydropic

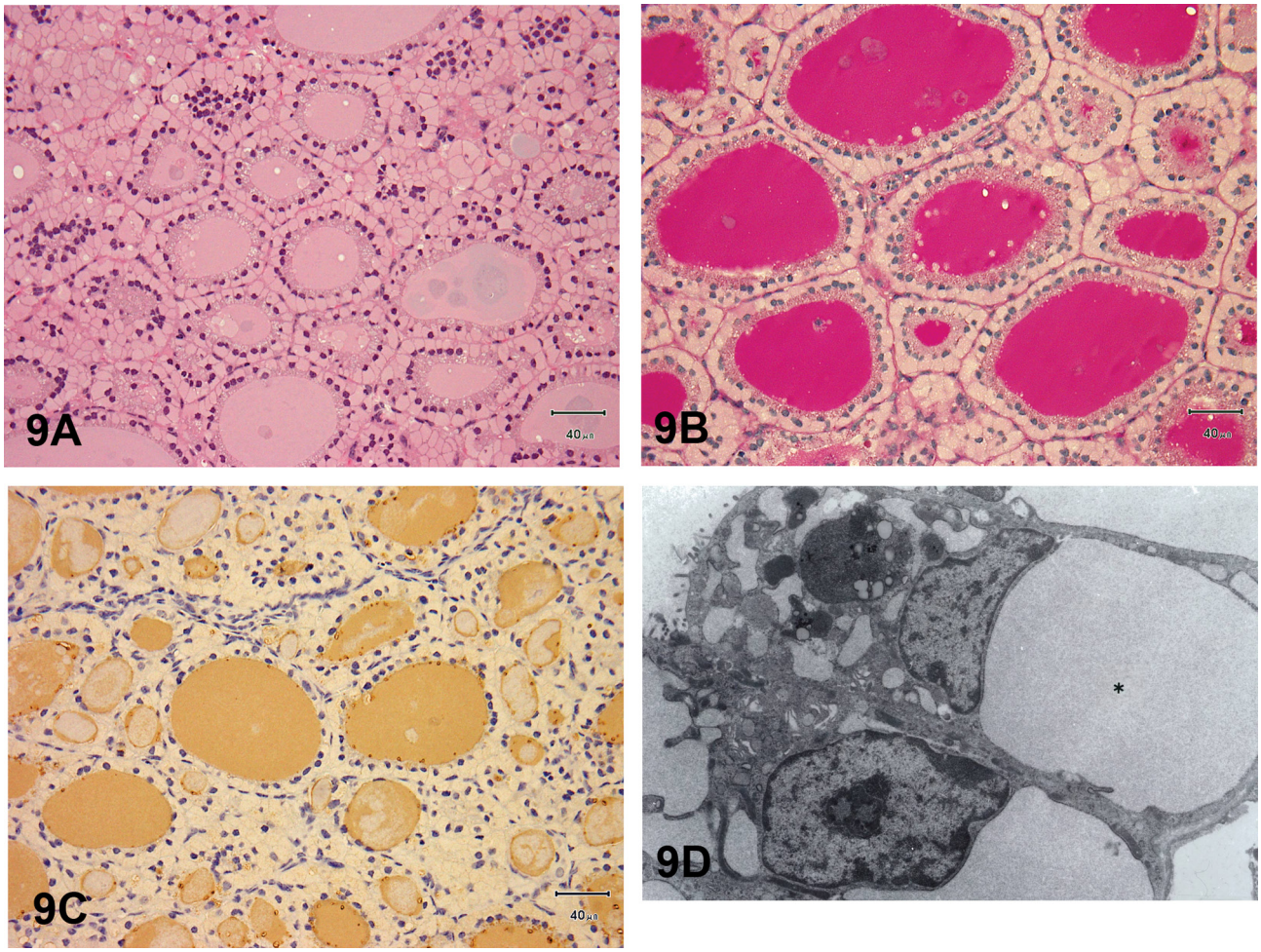

Fig. 9. Thyroid follicular cell degeneration in a cynomolgus monkey. A: Large vacuoles are observed in the basal region of each follicular epithelial cell, and the nuclei are characteristically located in the apical region adjacent to the follicular lumina. H & E staining. The scale bars indicate 40 μm. B: The colloid was positive, and the vacuoles were negative with PAS. The scale bars indicate 40 μm. C: The colloid reacted positively, and the vacuoles reacted negatively for thyroglobulin antibody. The scale bars indicate 40 μm. D: Electron micrographs of the thyroid follicular cells. In the basal portion, there is dilatation of the rough endoplasmic reticulum (RER), corresponding to the vacuoles (*) observed by light microscopy.

substances. In contrast to vacuolar degeneration, cellular hypertrophy is the increase in the volume of cells due to the proliferation of organelles. In general, hypertrophic cells have a centrally located prominent nucleus and nucleolus due to excessive protein synthesis. Other features of follicular hypertrophy include large cuboidal to columnar cells, a decrease in the diameter of the follicular lumens, decreased colloid eosinophilia, and increased number of follicles. This change is considered to be physiologic, that is, an early response of follicular cells to increased TSH secretion.

Large vacuoles at the basal region of the thyroid follicular epithelium have been reported in Fisher 344 rats and Wistar Hannover GALAS rats[55–57]. The vacuolar degeneration in the present case is very similar to the findings in reported rat cases in which the vacuoles reacted negatively to PAS and thyroglobulin[55, 58]. Dilatation of RER in follicular cells has also been reported in animals with genetic hypothyroidism[56, 57, 59–63]. Dilatation of the RER might be the process through which thyroid hormone synthesis or secretion was affected. In the present case, the plasma TSH, T3 and T4 levels of frozen samples were within the normal ranges, suggesting that the thyroid function remained intact. Furthermore, no abnormalities were seen in blood biochemistry, other organs or body weight. The animal was found to be healthy, and there were no adverse clinical observations. From these results, it is suggested that the function of the thyroid gland with vacuolar degeneration was maintained to a degree that still allowed the animal to remain in a healthy condition. It is uncertain whether vacuolar degeneration is part of a process that may lead to an adverse lesion or merely a morphological change that allows the cell to remain in a stable state. It is also unknown whether the change originated genetically or was brought about by other causes.

Feline Congenital Hepatic Fibrosis

Dr. Yasuhiro Tanaka of Setsunan University presented an unusual liver lesion in a 1-year-old female cat. There was a mild elevation of liver enzymes (AST, ALT), and a CT scan was performed, but no portal vein branch abnormality was detected. Macroscopically, the liver was normal in size, and irregular white spots were detected on the liver surface (Fig. 10A). A liver biopsy was performed to evaluate this abnormality.

The lesions were located in the portal areas, but the hepatic lobular structure was relatively normal (Fig. 10B). In the portal areas, significant bile duct hyperplasia was seen. As a characteristic change, bridging fibrosis with hyperplastic bile ducts connecting adjacent portal triads was present. In the liver parenchyma, only slight inflammatory cell infiltration and single cell necrosis were detected (Fig. 10C). In these lesions, fibrosis around the hyperplastic bile ducts was observed. Furthermore, portal vein hypoplasia and inflammatory cell infiltrates accompanied these lesions, but the inflammatory change was very slight (Fig. 10D). The hyperplastic bile ducts were dilated with irregularly shaped lumens, and luminal necrotic cells or cell debris were frequently observed. In addition, epithelial cells protruded into these bile duct lumens. However, cellular atypia was not present (Fig. 10E).

Therefore, the final characterization of this lesion was remarkable bile duct hyperplasia with an irregular shape, bridging fibrosis with a marked increase in irregularly shaped bile ducts, and a few inflammatory changes.

After presentation of this background information and viewing several macro- and microscopic images, a vote was taken for this case. The voting choices were 1) bile duct hyperplasia with hepatitis; 2) congenital hepatic fibrosis; 3) cholangitis, primary hypoplasia of the portal vein; 4) cholangiohepatitis; 5) cholangiofibrosis; 6) cholangiocellular adenoma; and 7) cholangiocellular carcinoma. The answer most favored by the audience was cholangiofibrosis (43%). In contrast, the presenter's diagnosis of congenital hepatic fibrosis (CHF) garnered only 10% of the votes.

After the voting was completed, the presenter showed a series of images that illustrated lesions of various livers with different causes for an inflammatory change, a neoplastic lesion, and a congenital anomaly. The reasons why the presenter judged this case as a congenital anomaly rather than a neoplastic change or an inflammatory change included 1) the fact that the inflammatory changes were very slight in the Glisson's capsule and liver parenchyma, 2) the fact that the shape of the hyperplastic bile duct was irregular, and 3) the fact that cellular atypia of the epithelial cells was not recognized.

To describe this lesion more fully, Dr. Tanaka showed illustrations of bile duct embryogenesis and ductal plate malformation as a congenital anomaly. The embryonic biliary precursor cells form a periportal sheet called the ductal plate, which is progressively remodeled to form the intrahepatic bile ducts. A limited number of ductal plate cells participate in duct formation; those not involved in duct development are believed to involute by apoptosis. The intrahepatic bile duct system is fully developed after birth. In the present case, there was abnormal bile duct development and differentiation, so the ductal plate remained around the portal vein[64–66]. When a large segment of the intrahepatic bile duct is affected, large cysts can be identified macroscopically. Caroli disease and polycystic liver disease are included in this category, and both are autosomal dominant or recessive conditions. On the other hand, when an intermediate segment of the intrahepatic bile duct is affected, the cysts cannot be easily identified macroscopically. CHF, also called juvenile polycystic disease, is such a case[67, 68]. CHF in humans in usually congenital, but sporadic cases have been reported. It is a fibrocystic liver disease associated with autosomal recessive polycystic kidney disease. In humans, as in this case, there is proliferation of interlobular bile ducts within the portal areas, with fibrosis that does not alter hepatic lobular architecture.

Finally, Dr. Tanaka showed that the lesion was consistent with the diagnostic features of CHF as described in the literature.

Macroscopic features

- Liver is normal in size without macroscopically visible cysts[69]
- Irregular white spots are confirmed on the liver surface[69]

Microscopic features

- Varying degrees of hepatic fibrosis with nodular formation[66]
- Bridging fibrosis with a marked increase of small or irregular bile duct profiles[70]
- Minimal to absent inflammation[67,70]
- Lack of nodular regeneration or other histological evidence of chronic hepatitis[70]

Middle Ear Adenocarcinoma in a Young Rat

Dr. Hiroko Kokoshima of Mitsubishi Chemical Medience Corp. presented a case of a tumor in the base of the skull of a 15-week-old Crl:CD(SD) male rat. This animal was in the low-dose group of a toxicity study. Although there were no clinical signs, there was a gross finding of a green mass at the right tympanic cavity. Histopathologically, this tumor was located from the right tympanic cavity to the side of the palate. Two different features were seen; one consisted of neoplastic cells forming tubule-like structures embedded in an abundant eosinophilic matrix (Fig. 11A), with the other consisting of a papillary proliferation of neoplastic cells with less eosinophilic matrix (Fig. 11B).

The voting choices for this tumor were (1) yolk sac carcinoma; (2) teratoma; (3) adenocarcinoma, middle ear; (4) adenocarcinoma, salivary gland; (5) other neoplasm; and (6) other nonneoplastic lesion. The top three choices were adenocarcinoma, middle ear (34%); yolk sac carcinoma (27%); and teratoma (18%), with a few votes for the other diagnoses.

Histopathologically, there were morphological simi-

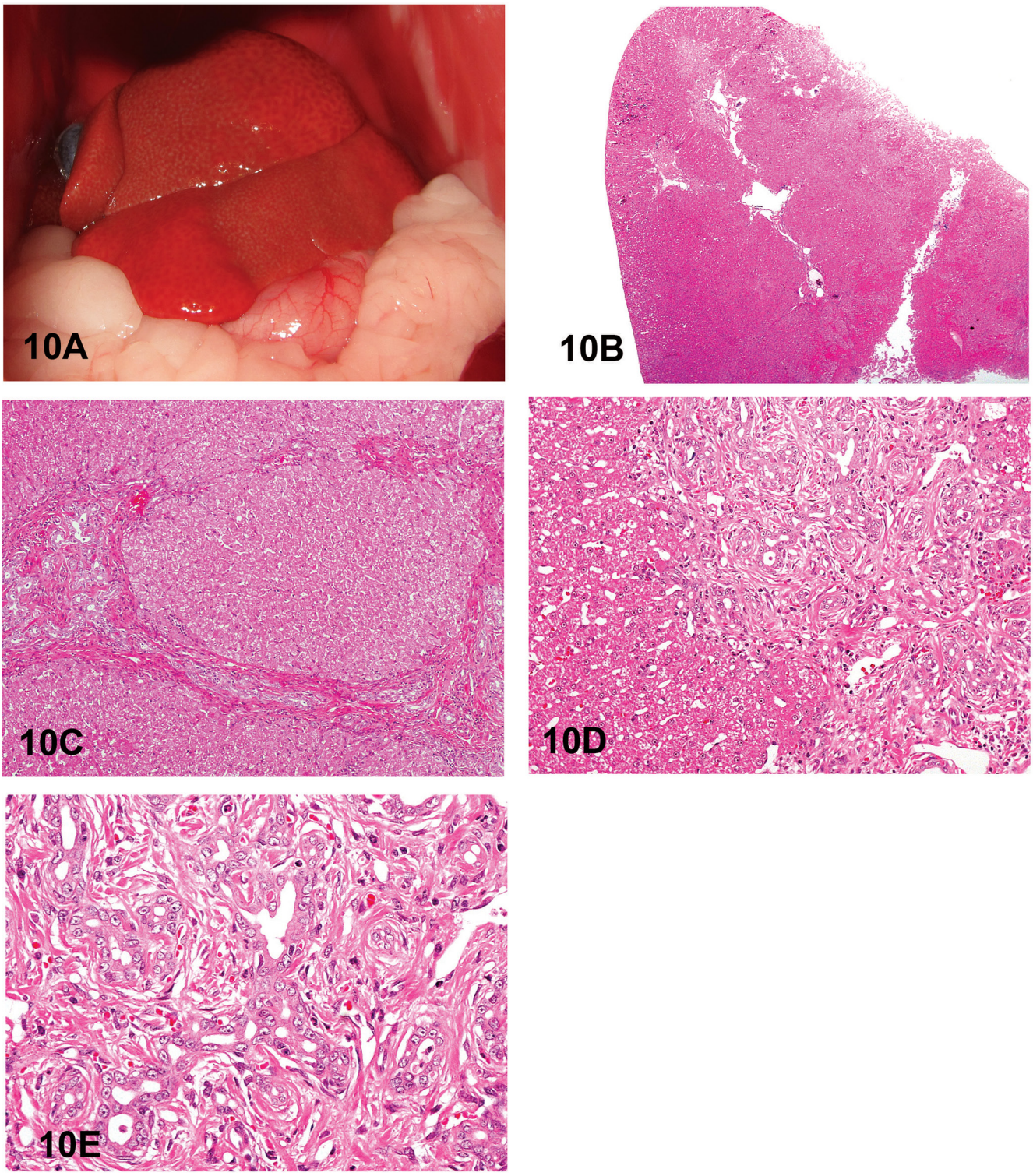

Fig. 10. Congenital hepatic fibrosis in a young cat. A: Macroscopic image of the liver of a 1-year-old female cat. B: The lesions are located in the portal areas, and Glisson's capsule is expanded by fibrous connective tissue. H & E staining, × 40. C: Bile duct hyperplasia and bridging fibrosis with hyperplastic bile ducts connecting adjacent portal triads. A few inflammatory changes are present in the liver parenchyma. H & E staining, × 100. D: Significant fibrosis around hyperplastic bile ducts and minimal inflammatory changes. H & E staining, × 200. E: Higher magnification of Fig. 10D. Irregularly shaped bile ducts, and intraluminal necrotic cells and cell debris. H & E staining, × 400.

larities between a yolk sac carcinoma and this neoplasm. The eosinophilic matrix and a part of the cytoplasm of some embedded neoplastic cells showed strong positivity for both PAS and laminin (Fig. 11C), which was quite similar to a yolk sac carcinoma. However, there were also some differences from yolk sac carcinoma. First, this neoplasm was

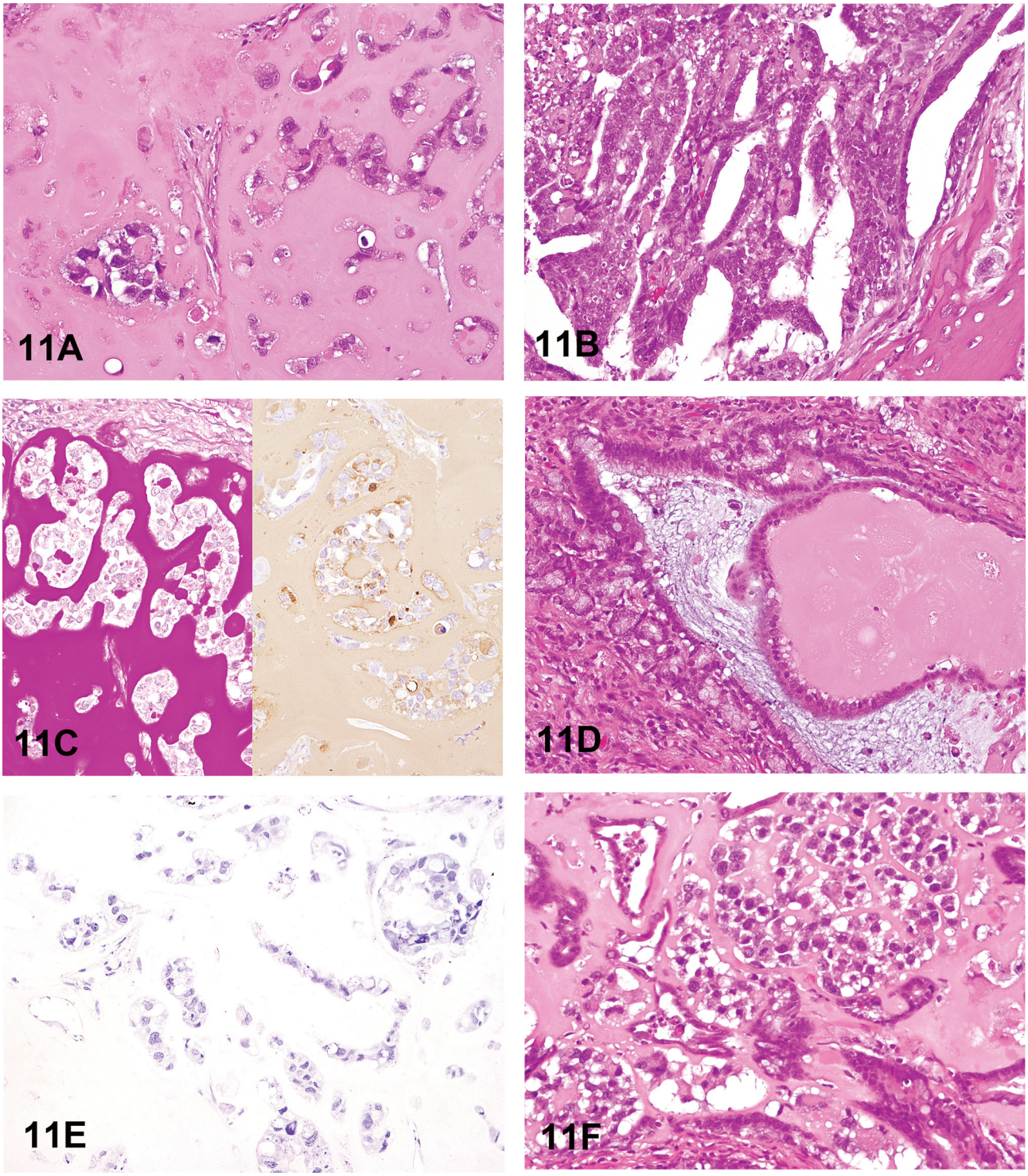

Fig. 11. Adenocarcinoma of the middle ear in a 15-week-old male Crl:CD(SD) rat with eosinophilic matrix. A: Neoplastic cells embedded in an abundant eosinophilic matrix. H & E staining, × 400. B: Papillary proliferation of the neoplastic cells. H & E staining, × 400. C: PAS staining (left) and immunohistochemistry for laminin (right). The eosinophilic matrix shows positive staining for both. × 400. D: Epithelial structure consisting of goblet cells and ciliated cells. H & E staining, × 400. E: The neoplastic cells embedded in the eosinophilic matrix are negative with AFP immunostaining, × 400. F: The association between the cells with an epithelial nature and the embedded cells. H & E staining, × 400.

located in the middle ear, not in the gonad. Furthermore, a part of the tympanic bone was seen in the periphery of the neoplasm, so the growth area was thought to be mainly in the tympanic cavity, where no germ cells exist. Secondly, strong mucous production was seen. Typically, yolk sac carcinoma cannot produce mucous. Thirdly, neoplastic cells

have an epithelial nature, with goblet cells and ciliated cells (Fig. 11D).

There were other features that were not consistent with a yolk sac carcinoma; neoplastic cells were negative with an immunohistochemical stain using anti- alphafetoprotein (AFP) antibody, whereas the liver and yolk sac of a 17-day old embryonic fetus are positive (Fig. 11E). Furthermore, in the electron microscopic examination, an amorphous matrix was seen in the interstitium and cytoplasm, but there was no characteristic feature such as a laminated structure suggesting yolk sac carcinoma[71].

The nature of the eosinophilic matrix was also discussed. The eosinophilic matrix was not amyloid due to negative Congo red staining. Other various stains, including Masson's trichrome and methenamine silver, could not identify the nature of this matrix.

The neoplastic cells embedded in the abundant eosinophilic matrix appeared to form glandular-like structures. Moreover, there was an association between the cells with an epithelial nature and the embedded cells (Fig. 11F). Mucous production was also seen in the embedded cells. So these two cells were thought to have the same origin; therefore, it was diagnosed as an adenocarcinoma.

The origin of this adenocarcinoma was ascertained to be the middle ear epithelium because of the location and morphological similarity to the middle ear epithelium, which is composed of ciliated and goblet cells. In humans, middle ear tumors are rare and generally considered benign. Histologically, middle ear tumors can have many different patterns, including solid, glandular or trabecular. Moreover, mucin production can occasionally be demonstrated[72]. There are a few reports concerning middle ear tumors in dogs[73, 74] and cats[75], but there have been no reports in the rat as far as we know. Interestingly, during the discussion period, one audience member noted that there have been rare reports of yolk sac carcinomas in the ears and tympanic parts of the temporal bones in humans[76, 77].

Cholangiofibrosis versus Cholangiosarcoma

Classical examples of hepatic cholangiomas and cholangiocarcinomas were presented by Dr. Robert Maronpot (Maronpot Consulting LLC, Raleigh, NC) immediately prior to presentation of controversial intrahepatic cholangial lesions consisting of proliferative and metaplastic changes with associated inflammation. These cholangial lesions have only been seen in treated rodents, primarily in rats, exposed to a variety of xenobiotics[78–81].

Cholangiofibrosis, and morphologically similar lesions that have been considered to be cholangiocarcinomas, represent a diagnostic challenge. The degree of liver involvement, even in a single animal, ranges from small subcapsular lesions to irregular patchy lesions with sparing of some lobes to almost total involvement of entire lobes (Fig. 12A).

With the exception of subcapsular lesions with extensive dilation of proliferative glandular structures (see 12G), cholangiofibrosis tends to be contractile rather than expansive, especially when viewed at low magnification. At high magnification, morphological features include dilated glandular structures lined by a single layer of epithelium. The glands are filled with necrotic debris and/or mucus, may contain neutrophils, are lined by sometimes an incomplete flattened to cuboidal to columnar epithelium including goblet and Paneth cells (intestinal metaplasia) and are surrounded by chronic active inflammation with prominent fibrosis (Figs. 12B and C). In some instances, the proliferative and inflammatory response is disseminated throughout the liver.

Dr. Maronpot pointed out that in the past the distinction between benign and malignant forms of this cholangial lesion has primarily been based on the extent of liver involvement in the absence of pathognostic morphological features. Unequivocal evidence for metastasis of these lesions has not been seen in a recent case. Dr. Maronpot believes that these proliferative and metaplastic, intrahepatic cholangial lesions are variations of benign cholangiofibrosis and, with rare exceptions, are not malignant neoplasms.

Following presentation of lesions previously diagnosed and confirmed by peer review to be either cholangiofibrosis or cholangiocarcinoma, Dr. Maronpot presented four cases for audience voting. In all cases, the voting choices were cholangioma, cystic cholangioma, cholangiocarcinoma, cholangiofibrosis and cystic cholangiofibrosis.

Case 1 from a treated female Sprague-Dawley rat was originally diagnosed as cholangiocarcinoma and had extensive involvement of hepatic parenchyma with active glandular formation at the lesion perimeter (Fig. 12D). The audience vote was 75% in favor of cholangiofibrosis with 19% choosing cholangiocarcinoma. Case 2 was a lesion with extensive glandular proliferation involving greater than 90% of the hepatic parenchyma from an F344/N rat exposed to high-dose estragole for 90 days (Fig. 12E). Based on the extensive parenchymal involvement, this lesion was originally diagnosed as a cholangiocarcinoma. The audience voting favored a diagnosis of cholangiofibrosis (57%) with 38% voting for cholangiocarcinoma. Case 3 was a lesion characterized by solid sheets of proliferating biliary cells with some dilated, metaplastic glands from an F344/N rat given high-dose furan for 90 days (Fig. 12F). The original diagnosis was cholangiofibrosis, but the solid cell sheets influenced 70% of the audience to select cholangiocarcinoma. Case 4, from a treated female Sprague-Dawley rat, was a small lesion characterized by dilated, mucus-filled glands on the liver surface (Fig. 12G). This lesion was originally diagnosed as a cholangiofibrotic nodule; the majority of the audience (61%) voted for cystic cholangiofibrosis with 19% in favor of cholangiofibrosis and 12% favoring cystic cholangioma.

In conclusion, with the exception of Case 3, audience opinion favored a diagnosis of cholangiofibrosis for hepatic cholangial lesions characterized by proliferative and metaplastic biliary glands with associated inflammation.

Acknowledgements: The authors wish to thank Dr. Haruka Horiuchi of DuPont Kabushiki Kaisha, Tokyo, Japan, and staff at Procom International Co., Ltd. of Tokyo, Japan, for

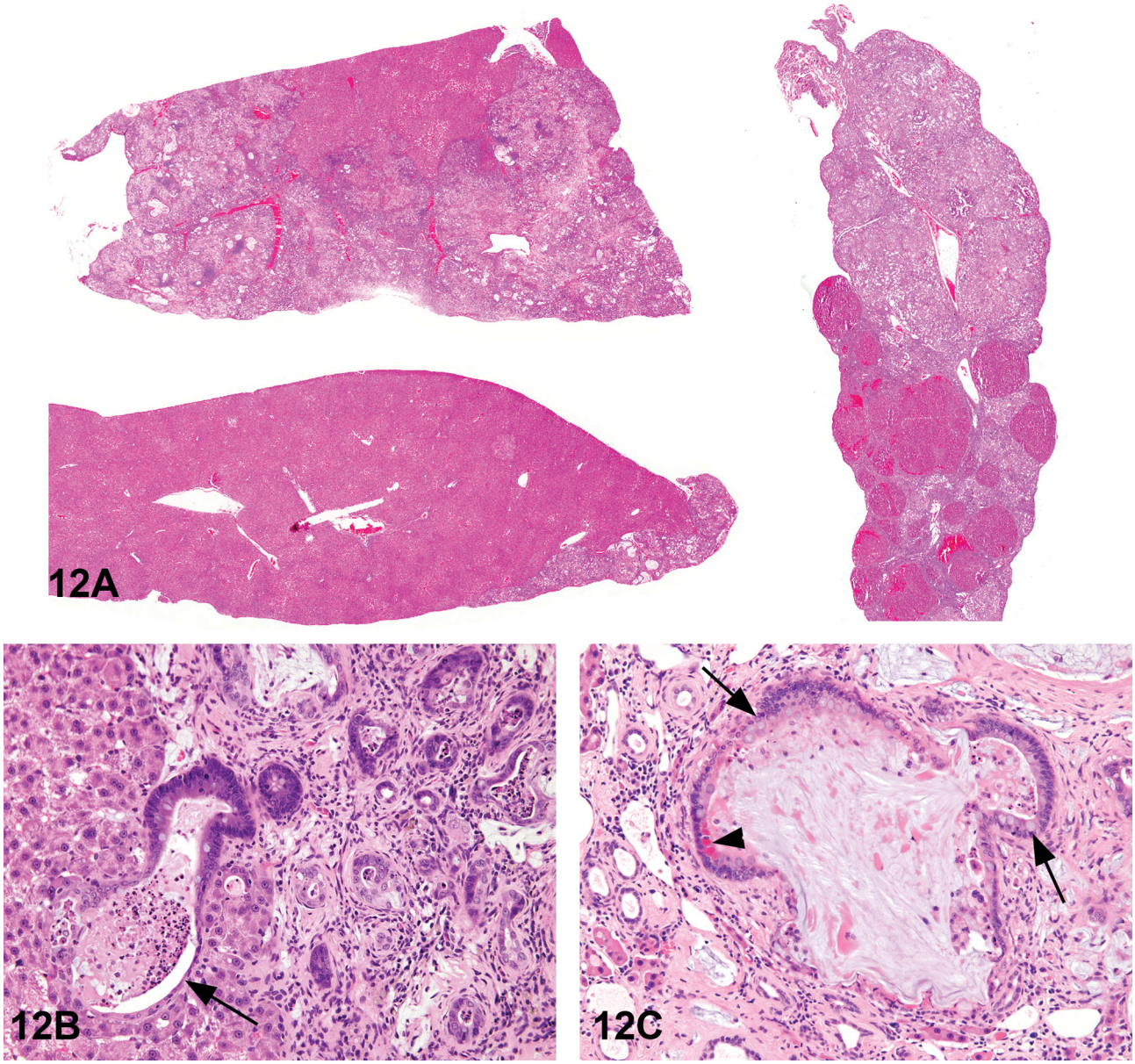

Fig. 12. Cholangiofibrosis versus cholangiocarcinoma. A: Low-magnification photomicrographs showing the variable extent of cholangial lesions in different lobes from a treated rat. H & E staining. B: Irregular and cystic gland formation and associated inflammation in the liver of a treated rat. Necrotic neutrophils and debris are present in a dilated gland that is incompletely lined by a hyperbasophilic columnar epithelium (arrow). H & E staining. C: A dilated, mucus-filled gland is surrounded by a chronic inflammatory response in the liver of a treated rat. The low cuboidal epithelium contains goblet cells (arrows) and Paneth cells (arrowhead). H & E staining. D: Representative photomicrograph from Case 1 showing a typical cholangiofibrotic response in a treated rat. There is extensive lobe involvement present in the low-magnification view (see inset). H & E staining. E: Representative photomicrograph from Case 2 showing a high magnification of hyperbasophilic cholangial cells surrounded by a chronic inflammatory reaction. Isolated trapped hepatocytes are present in the inflammatory matrix (arrows). A low magnification of the affected liver lobe is presented in the inset. H & E staining. F: An irregular glandular proliferative response with minimal inflammatory reaction is present in this treated rat. The proliferating cholangial cells are arranged in poorly demarcated nests and sheets with some glandular formation. This cholangial lesion, which represents only a portion of a liver lobe (see inset), was voted malignant by the voting majority. H & E staining. G: A small protruding cystic lesion (see inset) consisted of mucus-filled dilated glands surrounded by thick bands of connective tissue. H & E staining.

assistance with audiovisual needs. We greatly appreciate contributions by the Conference of Experimental Animal Histopathology (CEAH). Appreciation also goes to Ms. Elizabeth Ney of the NIEHS for her unique and creative cover artwork for the Symposium handouts.

Dr. Tsuchiya would like to express deepest gratitude to Drs. Izawa and Tanaka of Veterinary Pathology, Osaka Prefecture University for their enormous support with the electron microscopic analysis and insightful comments. Special thanks also go to members of Kansai Conference

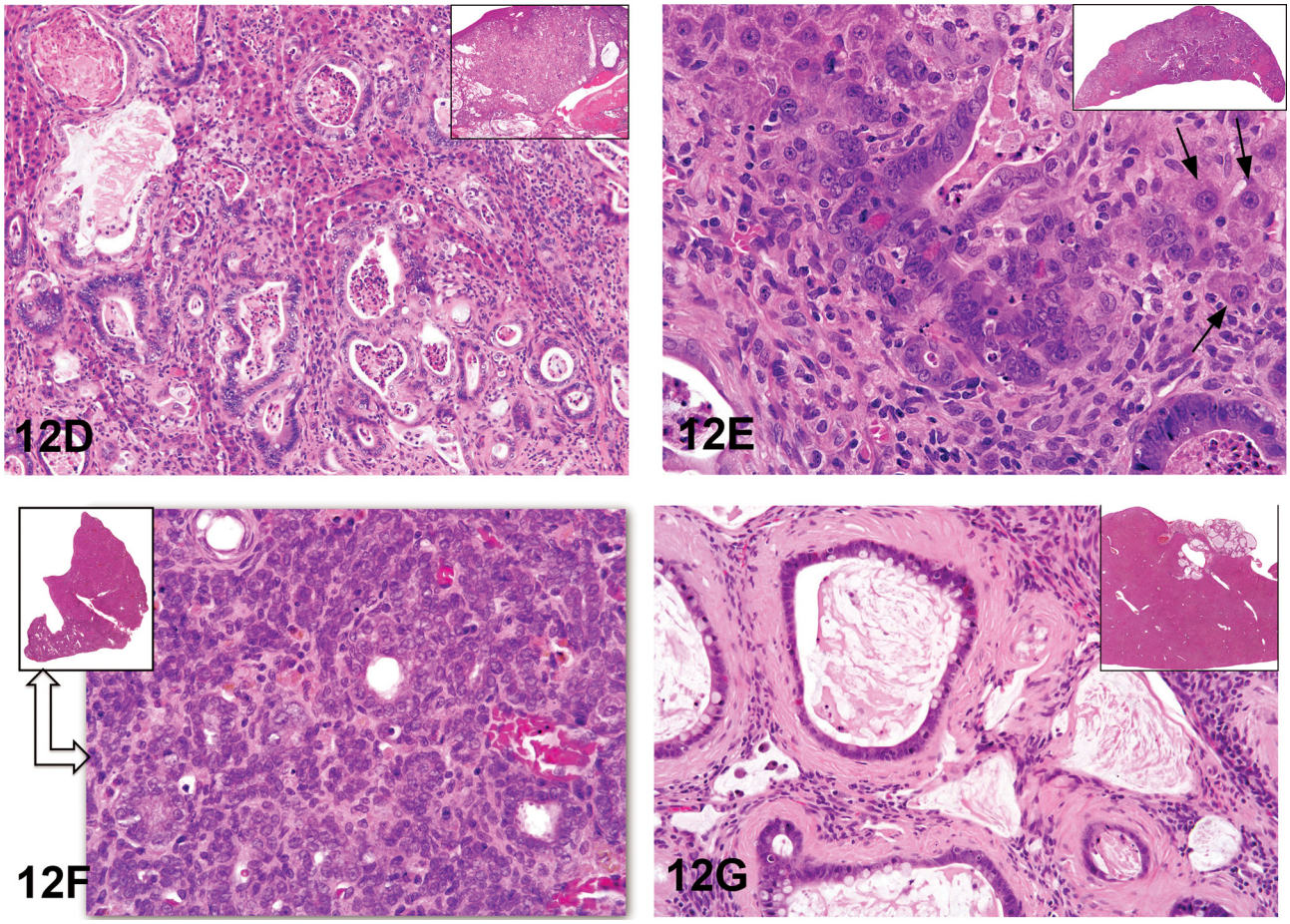

of Toxicological Pathology for their constructive comments and discussion. Dr. Hoenerhoff would like to acknowledge Dr. Jerrold Rehg of Saint Jude's Children's Research Hospital for supplying the CHI3L3 antibody and the NIEHS Immunohistochemistry Core Lab for their technical expertise.

This research was supported [in part] by the Intramural Research Program of the National Institutes of Health (NIH), National Institute of Environmental Health Sciences (NIEHS). This article may be the work product of an employee or group of employees of the NIEHS, NIH; however, the statements, opinions or conclusions contained herein do not necessarily represent the statements, opinions or conclusions of the NIEHS, NIH or United States government. We also express our thanks for the financial support of the JSTP for publication of these proceedings in the Journal of Toxicologic Pathology.

Figures 1 C–F, H, 5A–F, 6C–H and 8A–L were reprinted with permission from Elmore *et al.*, Toxicologic Pathology, 41: 151–180, 2013. Figures 4 A, B, D and E were reprinted with permission from Adams *et al.*, Toxicologic Pathology, 39: 240–266, 2011. Figures 7A–F were reprinted with permission from Kouchi *et al.*, Toxicologic Pathology, 39: 975–979, 2011. Figures 9B–D were reprinted with permission from Hatakeyama *et al.*, Journal of Toxicologic Pathology, 24: 229–232, 2011.

References

1. Elmore SA, Berridge BR, Boyle MC, Cora MC, Hoenerhoff MJ, Kooistra L, Laast VA, Morrison JP, Rao D, Rinke M, and Yoshizawa K. Proceedings of the 2012 national toxicology program satellite symposium. Toxicol Pathol. **41**: 151–180. 2013. [Medline]
2. Boorman G, Crabbs TA, Kolenda-Roberts H, Latimer K, Miller AD, Muravnick KB, Nyska A, Ochoa R, Pardo ID, Ramot Y, Rao DB, Schuh J, Suttie A, Travlos GS, Ward JM, Wolf JC, and Elmore SA. Proceedings of the 2011 National Toxicology Program Satellite Symposium. Toxicol Pathol. **40**: 321–344. 2012. [Medline]
3. Adams ET, Auerbach S, Blackshear PE, Bradley A, Gruebbel MM, Little PB, Malarkey D, Maronpot R, McKay JS, Miller RA, Moore RR, Morrison JP, Nyska A, Ramot Y, Rao D, Suttie A, Wells MY, Willson GA, and Elmore SA. Proceedings of the 2010 National Toxicology Program Satellite Symposium. Toxicol Pathol. **39**: 240–266. 2011. [Medline]
4. Bach U, Hailey JR, Hill GD, Kaufmann W, Latimer KS, Malarkey DE, Maronpot RM, Miller RA, Moore RR, Morrison JP, Nolte T, Rinke M, Rittinghausen S, Suttie AW, Travlos GS, Vahle JL, Willson GA, and Elmore SA. Proceedings of the 2009 National Toxicology Program Satellite Symposium. Toxicol Pathol. **38**: 9–36. 2010. [Medline]
5. Seok JH, Ahn K, and Park HJ. Diffusion MRI findings of

cytomegalovirus-associated ventriculitis: a case report. Br J Radiol. **84**: e179–e181. 2011. [Medline]
6. Matsukawa T, Goto H, Takahashi K, Asanuma S, Yasumoto A, Takahata M, Shigematsu A, Endo T, Tanaka J, Hashino S, Tanaka S, and Imamura M. A fatal case of cytomegalovirus ventriculoencephalitis in a mycosis fungoides patient who received multiple umbilical cord blood cell transplantations. Int J Hematol. **95**: 217–222. 2012. [Medline]
7. Weiss SW, and Goldblum JR. Soft Tissue Tumors, 5th ed, Mosby Elsevier, Philadelphia, 853-887. 2007.
8. Pumarola M, Anor S, Borras D, and Ferrer I. Malignant epithelioid schwannoma affecting the trigeminal nerve of a dog. Vet Pathol. **33**: 434–436. 1996. [Medline]
9. Laskin WB, Fetsch JF, Lasota J, and Miettinen M. Benign epithelioid peripheral nerve sheath tumors of the soft tissues: clinicopathologic spectrum of 33 cases. Am J Surg Pathol. **29**: 39–51. 2005. [Medline]
10. McMenamin ME, and Fletcher CD. Expanding the spectrum of malignant change in schwannomas: epithelioid malignant change, epithelioid malignant peripheral nerve sheath tumor, and epithelioid angiosarcoma: a study of 17 cases. Am J Surg Pathol. **25**: 13–25. 2001. [Medline]
11. Doi T, Kokoshima H, Kanno T, Sato J, Wako Y, Tsuchitani M, and Matsui T. New findings concerning eosinophilic substance deposition in mouse nasal septum: sex difference and no increase in seniles. Toxicol Pathol. **38**: 631–636. 2010. [Medline]
12. Doi T, Kotani Y, Kokoshima H, Kanno T, Wako Y, and Tsuchitani M. Eosinophilic substance is "not amyloid" in the mouse nasal septum. Vet Pathol. **44**: 796–802. 2007. [Medline]
13. Doi T, Kotani Y, Kokoshima H, Kanno T, Wako Y, Tsuchitani M, and Matsui T. Deposition process of eosinophilic substance in mouse nasal septum. J Vet Med Sci. **71**: 931–935. 2009. [Medline]
14. Renne R, Brix A, Harkema J, Herbert R, Kittel B, Lewis D, March T, Nagano K, Pino M, Rittinghausen S, Rosenbruch M, Tellier P, and Wohrmann T. Proliferative and nonproliferative lesions of the rat and mouse respiratory tract. Toxicol Pathol. **37**: 5S–73S. 2009. [Medline]
15. Hosotani R, Ida J, Kogire M, Fujimoto K, Doi R, and Imamura M. Expression of pancreatic duodenal hoemobox-1 in pancreatic islet neogenesis after surgical wrapping in rats. Surgery. **135**: 297–306. 2004. [Medline]
16. Hansen JF. Ross. PE, Makovec GT. Eustis SL, and Sigler RE. Proliferative and other selected lesions of the exocrine pancreas in rats, GI-6. In: Guides for Toxicologic Pathology. STP/ARP/AF1P, Washington, DC. 1995.
17. Riley MGI, Boonnan GA, McDonald MM, Lognecker D, Solleveld HA, and Giles HD. Proliferative and metaplaslic lesions of the endocrine pancreas in rats, E-1. In: Guides for Toxicologic Pathology. STP/ARP/AFIP, Washington, D.C. 1990.
18. goRENI. The standard reference for nomenclature and diagnostic criteria in toxicologic pathology. Website: http://www.goreni.org/.
19. Yoshizawa K, Uehara N, Kimura A, Emoto Y, Kinoshita Y, Yuri T, Takada H, Moriguchi T, Hamazaki T, and Tsubura A. Promoting effect of arachidonic acid supplementation on *N*-methyl-*N*-nitrosourea-induced pancreatic acinar cell hyperplasia in young Lewis rats. Oncol Lett. **5**: 76–82. 2013. [Medline]
20. Murray AB, and Luz A. Acidophilic macrophage pneumonia in laboratory mice. Vet Pathol. **27**: 274–281. 1990. [Medline]
21. Guo L, Johnson RS, and Schuh JC. Biochemical characterization of endogenously formed eosinophilic crystals in the lungs of mice. J Biol Chem. **275**: 8032–8037. 2000. [Medline]
22. Webb DC, McKenzie AN, and Foster PS. Expression of the Ym2 lectin-binding protein is dependent on interleukin (IL)-4 and IL-13 signal transduction: identification of a novel allergy-associated protein. J Biol Chem. **276**: 41969–41976. 2001. [Medline]
23. Zhao J, Zhu H, Wong CH, Leung KY, and Wong WS. Increased lungkine and chitinase levels in allergic airway inflammation: a proteomics approach. Proteomics. **5**: 2799–2807. 2005. [Medline]
24. Hung SI, Chang AC, Kato I, and Chang NC. Transient expression of Ym1, a heparin-binding lectin, during developmental hematopoiesis and inflammation. J Leukoc Biol. **72**: 72–82. 2002. [Medline]
25. Matulionis DH, and Yokel RA. Murine lung response to kaolin conveyed by cigarette smoke. Virchows Arch A Pathol Anat Histopathol. **413**: 227–237. 1988. [Medline]
26. Feldmesser M, Kress Y, and Casadevall A. Intracellular crystal formation as a mechanism of cytotoxicity in murine pulmonary *Cryptococcus neoformans* infection. Infect Immun. **69**: 2723–2727. 2001. [Medline]
27. Sato H, Kawase S, Oku Y, Kamiya M, and Ohbayashi M. Acidophilic protein crystals in lungs and bile ducts of helminth-infected mice. Nihon Juigaku Zasshi. **50**: 299–302. 1988. [Medline]
28. Takamoto M, Ovington KS, Behm CA, Sugane K, Young IG, and Matthaei KI. Eosinophilia, parasite burden and lung damage in Toxocara canis infection in C57Bl/6 mice genetically deficient in IL-5. Immunology. **90**: 511–517. 1997. [Medline]
29. Harbord M, Novelli M, Canas B, Power D, Davis C, Godovac-Zimmermann J, Roes J, and Segal AW. Ym1 is a neutrophil granule protein that crystallizes in p47phox-deficient mice. J Biol Chem. **277**: 5468–5475. 2002. [Medline]
30. Hoenerhoff MJ, Starost MF, and Ward JM. Eosinophilic crystalline pneumonia as a major cause of death in 129S4/SvJae mice. Vet Pathol. **43**: 682–688. 2006. [Medline]
31. Ward JM, Yoon M, Anver MR, Haines DC, Kudo G, Gonzalez FJ, and Kimura S. Hyalinosis and Ym1/Ym2 gene expression in the stomach and respiratory tract of 129S4/SvJae and wild-type and CYP1A2-null B6, 129 mice. Am J Pathol. **158**: 323–332. 2001. [Medline]
32. France MP, and Muir D. An outbreak of pulmonary mycosis in respiratory burst-deficient (gp91(phox-/-)) Mice with concurrent acidophilic macrophage pneumonia. J Comp Pathol. **123**: 190–194. 2000. [Medline]
33. Liu Q, Cheng LI, Yi L, Zhu N, Wood A, Changpriroa CM, Ward JM, and Jackson SH. p47phox deficiency induces macrophage dysfunction resulting in progressive crystalline macrophage pneumonia. Am J Pathol. **174**: 153–163. 2009. [Medline]
34. Shultz LD, Coman DR, Bailey CL, Beamer WG, and Sidman CL. "Viable motheaten," a new allele at the motheaten locus. I. Pathology. Am J Pathol. **116**: 179–192. 1984. [Medline]
35. Ward JM. Pulmonary pathology of the motheaten mouse.

Vet Pathol. **15**: 170–178. 1978. [Medline]
36. Chang NC, Hung SI, Hwa KY, Kato I, Chen JE, Liu CH, and Chang AC. A macrophage protein, Ym1, transiently expressed during inflammation is a novel mammalian lectin. J Biol Chem. **276**: 17497–17506. 2001. [Medline]
37. Nio J, Fujimoto W, Konno A, Kon Y, Owhashi M, and Iwanaga T. Cellular expression of murine Ym1 and Ym2, chitinase family proteins, as revealed by in situ hybridization and immunohistochemistry. Histochem Cell Biol. **121**: 473–482. 2004. [Medline]
38. Nair MG, Cochrane DW, and Allen JE. Macrophages in chronic type 2 inflammation have a novel phenotype characterized by the abundant expression of Ym1 and Fizz1 that can be partly replicated in vitro. Immunol Lett. **85**: 173–180. 2003. [Medline]
39. Waern I, Jia J, Pejler G, Zcharia E, Vlodavsky I, Li JP, and Wernersson S. Accumulation of Ym1 and formation of intracellular crystalline bodies in alveolar macrophages lacking heparanase. Mol Immunol. **47**: 1467–1475. 2010. [Medline]
40. Marchesi F, Monestiroli SV, Capillo M, Gobbi A, Minucci S, Pelicci PG, and Scanziani E. Eosinophilic crystals as a distinctive morphologic feature of a hyaline droplet nephropathy in a mouse model of acute myelogenous leukaemia. J Vet Med A Physiol Pathol Clin Med. **50**: 103–107. 2003. [Medline]
41. Nathaniel DR. Paracrystalline arrays in atypical cristae and mitochondrial division. J Cell Sci. **42**: 23–32. 1980. [Medline]
42. Suski J, Lebiedzinska M, Machado NG, Oliveira PJ, Pinton P, Duszynski J, and Wieckowski MR. Mitochondrial tolerance to drugs and toxic agents in ageing and disease. Curr Drug Targets. **12**: 827–849. 2011. [Medline]
43. Svoboda DJ, and Manning RT. Chronic alcoholism with fatty metamorphosis of the liver. Mitochondrial alterations in hepatic cells. Am J Pathol. **44**: 645–662. 1964. [Medline]
44. Wojcinski ZW, Albassam MA, and Smith GS. Hyaline glomerulopathy in B6C3F1 mice. Toxicol Pathol. **19**: 224–229. 1991. [Medline]
45. National Toxicology Program Toxicology and carcinogenesis studies of pulegone (CAS No. 89-82-7) in F344/N rats and B6C3F1 mice (gavage studies). Natl Toxicol Program Tech Rep Ser. **563:** 1-201. 2011. Website: http://ntp.niehs.nih.gov/ntp/htdocs/LT_rpts/TR563.pdf#search=pulegone.
46. Kobayashi K, Sano F, Mutai M, and Sugimoto J. Glomerulonephritis with fibrillary deposition in a transgenic mouse carrying the human prototype c-Ha-ras gene (rasH2 mouse). Toxicol Pathol. **28**: 359–362. 2000. [Medline]
47. D'Agati VD, Jennette JC, and Silva FG. Non-neoplastic kidney diseases. In: An Atlas of Nontumor Pathology, ARP Press, Silver Spring, MD, Washington, DC. 225-230. 2005.
48. Iskandar SS, and Herrera GA. Glomerulopathies with organized deposits. Semin Diagn Pathol. **19**: 116–132. 2002. [Medline]
49. Korbet SM, Schwartz MM, Rosenberg BF, Sibley RK, and Lewis EJ. Immunotactoid glomerulopathy. Medicine (Baltimore). **64**: 228–243. 1985. [Medline]
50. Rosenstock JL, Markowitz GS, Valeri AM, Sacchi G, Appel GB, and D'Agati VD. Fibrillary and immunotactoid glomerulonephritis: Distinct entities with different clinical and pathologic features. Kidney Int. **63**: 1450–1461. 2003. [Medline]
51. Goldfarb S, Pugh TD, Koen H, and He YZ. Preneoplastic and neoplastic progression during hepatocarcinogenesis in mice injected with diethylnitrosamine in infancy. Environ Health Perspect. **50**: 149–161. 1983. [Medline]
52. Koen H, Pugh TD, and Goldfarb S. Centrilobular distribution of diethylnitrosamine-induced hepatocellular foci in the mouse. Lab Invest. **49**: 78–81. 1983. [Medline]
53. Thoolen B, Maronpot RR, Harada T, Nyska A, Rousseaux C, Nolte T, Malarkey DE, Kaufmann W, Kuttler K, Deschl U, Nakae D, Gregson R, Vinlove MP, Brix AE, Singh B, Belpoggi F, and Ward JM. Proliferative and nonproliferative lesions of the rat and mouse hepatobiliary system. Toxicol Pathol. **38**: 5S–81S. 2010. [Medline]
54. Hatakeyama H, Takei Y, Cruz Y, Miyoshi S, Watanabe J, Koizumi H, Shimoi A, and Satoh H. Spontaneous vacuolar degeneration of the thyroid follicular epithelium in cynomolgus monkeys. J Toxicol Pathol. **24**: 229–232. 2011. [Medline]
55. Shimoi A, Kuwayama C, Miyauchi M, Kakinuma C, Kamiya M, Harada T, Ogihara T, Kurokawa M, and Mizuguchi K. Vacuolar change in the thyroid follicular cells in BrlHan: WIST@Jcl (GALAS) rats. J Toxicol Pathol. **14**: 253–257. 2001.
56. Doi T, Namiki M, Ashina M, Toyota N, Kokoshima H, Kanno T, Wako Y, Tayama M, Nakashima Y, Nasu M, and Tsuchitani M. Morphological and endocrinological characteristics of the endocrine systems in Wistar Hannover GALAS rats showing spontaneous dwarfs. J Toxicol Pathol. **17**: 197–203. 2004.
57. Weber K, Ernst R, Fankhauser H, Hardisty JF, Heider W, and Stevens K. Thyroid dysplasia in Wistar Hannover GALAS rats. J Toxicol Pathol. **22**: 247–254. 2009. [Medline]
58. Takaoka M, Yamoto T, Teranishi M, Manabe S, and Goto N. A case of intracytoplasmic edema of follicular epithelial cells in rat thyroid. J Vet Med Sci. **56**: 989–991. 1994. [Medline]
59. Stein SA, Shanklin DR, Krulich L, Roth MG, Chubb CM, and Adams PM. Evaluation and characterization of the hyt/hyt hypothyroid mouse. II. Abnormalities of TSH and the thyroid gland. Neuroendocrinology. **49**: 509–519. 1989. [Medline]
60. Sakai Y, Yamashina S, and Furudate SI. Missing secretory granules, dilated endoplasmic reticulum, and nuclear dislocation in the thyroid gland of rdw rats with hereditary dwarfism. Anat Rec. **259**: 60–66. 2000. [Medline]
61. Mayerhofer A, Amador AG, Beamer WG, and Bartke A. Ultrastructural aspects of the goiter in cog/cog mice. J Hered. **79**: 200–203. 1988. [Medline]
62. Codaccioni JL, Carayon P, Michel-Bechet M, Foucault F, Lefort G, and Pierron H. Congenital hypothyroidism associated with thyrotropin unresponsiveness and thyroid cell membrane alterations. J Clin Endocrinol Metab. **50**: 932–937. 1980. [Medline]
63. Ohyama Y, Hosoya T, Kameya T, Suzuki N, Nakamura S, Kazahari K, Shibayama K, Yokota Y, and Matsuura N. Congenital euthyroid goitre with impaired thyroglobulin transport. Clin Endocrinol (Oxf). **41**: 129–135. 1994. [Medline]
64. Johnson CA, Gissen P, and Sergi C. Molecular pathology and genetics of congenital hepatorenal fibrocystic syndromes. J Med Genet. **40**: 311–319. 2003. [Medline]
65. Antoniou A, Raynaud P, Cordi S, Zong Y, Tronche F,

Stanger BZ, Jacquemin P, Pierreux CE, Clotman F, and Lemaigre FP. Intrahepatic bile ducts develop according to a new mode of tubulogenesis regulated by the transcription factor SOX9. Gastroenterology. **136**: 2325–2333. 2009. [Medline]
66. Shorbagi A, and Bayraktar Y. Experience of a single center with congenital hepatic fibrosis: a review of the literature. World J Gastroenterol. **16**: 683–690. 2010. [Medline]
67. Nakanuma Y, and Sato Y. Kannaitankan no keisei ijou - Tannou nouhousei kan-ahikkan to aentensei kan-senishou + Caroli-byou wo cyuusin ni. Kanzo. **44**: 619–631. 2003; (In Japanese).
68. Van den lngh T, Cullen JM, Twedt DC, Winkle TV, Desmet VJ, and Rothuizen J. Morphological classification of biliary disorders of the canine ond feline liver. In: WSAVA Standards for Clinical and Histological Diagnosis of Canine and Feline Liver Diseases. WSAVA Liver Standardization Group. Saunders Elsevier, Spain. 61-76. 2006.
69. Desmet VJ. Ludwig symposium on biliary disorders - part I. Pathogenesis of ductal plate abnormalities. Mayo Clin Proc. **73**: 80–89. 1998. [Medline]
70. Brown DL, Van Winkle T, Cecere T, Rushton S, Brachelente C, and Cullen JM. Congenital hepatic fibrosis in 5 dogs. Vet Pathol. **47**: 102–107. 2010. [Medline]
71. Sobis H. Yolk sac carcinoma. In: Monographs on the Pathology of Laboratory Animals 'Genital System', U Mohr and RD Hunt (eds). Springer-Verlag, Berlin. 127-134. 1987.
72. Lott Limbach AA, Hoschar AP, Thompson LD, Stelow EB, and Chute DJ. Middle ear adenomas stain for two cell populations and lack myoepithelial cell differentiation. Head Neck Pathol. **6**: 345–353. 2012. [Medline]
73. Little CJ, Pearson GR, and Lane JG. Neoplasia involving the middle ear cavity of dogs. Vet Rec. **124**: 54–57. 1989. [Medline]
74. Hargis AM, and Thomassen RW. Adenoma of the epithelium lining the eustachian tube in a beagle dog. Vet Pathol. **17**: 238–240. 1980. [Medline]
75. Lucroy MD, Vernau KM, Samii VF, and LeCouteur RA. Middle ear tumours with brainstem extension treated by ventral bulla osteotomy and craniectomy in two cats. Vet Comp Oncol. **2**: 234–242. 2004. [Medline]
76. Kaveti V, Sanjay R, and Ganeshula S. Yolk sac tumor of the ear: uncommon presentation of a rare tumor. J Clin Oncol. **28**: e349–e350. 2010. [Medline]
77. Fukunaga M, Miyazawa Y, Harada T, Ushigome S, and Ishikawa E. Yolk sac tumour of the ear. Histopathology. **27**: 563–567. 1995. [Medline]
78. Bannasch P, and Zerban H. Pathology of tumours in laboratory animals. In: Tumours of the rat. Tumours of the liver. IARC Sci Publ. 199-240. 1990.
79. Eustis S, Boorman G, Harada T, and Popp J. Liver. In: Pathology of the Fischer Rat. Reference and Atlas., G Boorman, S Eustis, M Elwell, CA Montgomery, Jr., and W MacKenzie (eds). Academic Press, San Diego. 71-94. 1990.
80. Kimbrough RD, Linder RE, Burse VW, and Jennings RW. Adenofibrosis in the rat liver with persistence of polychlorinated biphenyls in adipose tissue. Arch Environ Health. **27**: 390–395. 1973. [Medline]
81. Hailey JR, Walker NJ, Sells DM, Brix AE, Jokinen MP, and Nyska A. Classification of proliferative hepatocellular lesions in Harlan sprague-dawley rats chronically exposed to dioxin-like compounds. Toxicol Pathol. **33**: 165–174. 2005. [Medline]